2 mil

Third Semi-Annual Report
National Aeronautics and Space Administration
Lewis Research Center
Grant NGR 23-004-068

PRELIMINARY RESULTS FOR A LARGE ANGLE OBLIQUE JET IMPINGEMENT AND FLOW AND FOR THE EFFECT OF INITIAL CONDITIONS ON THE NEAR FIELD OF AN AXISYMMETRIC JET

prepared by

John F. Foss
Stanley J. Kleis

Division of Engineering Research
MICHIGAN STATE UNIVERSITY
East Lansing, Michigan 48823
May 25, 1973

Third Semi-Annual Report
National Aeronautics and Space Administration
Lewis Research Center
Grant NGR 23-004-068

PRELIMINARY RESULTS FOR A LARGE ANGLE OBLIQUE JET IMPINGEMENT AND FLOW AND FOR THE EFFECT OF INITIAL CONDITIONS ON THE NEAR FIELD OF AN AXISYMMETRIC JET

prepared by

John F. Foss
Stanley J. Kleis

Division of Engineering Research
MICHIGAN STATE UNIVERSITY
East Lansing, Michigan 48823
May 25. 1973

ABSTRACT

The structure of an axisymmetric jet in the near field ($0 \leq x/d <$ self preserving region) is of importance to the National Aeronautics and Space Administration mission in aerodynamics. It is this region of the jet which is primarily responsible for jet noise and the jet impingement schemes for STOL aircraft involve this region of the jet flow.

It is inferred from previous studies, and the inference is supported by analysis, that the scale and intensity of the turbulence structure at the jet exit plane are the important boundary conditions which effect the development of the flow in the near field.

The techniques to study these effects while maintaining a uniform mean flow and the results which document the range of the initial conditions are presented herein.

The large angle, oblique jet impingement condition is of interest in terms of the jet/flap interaction. The technological problem involves angles of 30 and 60 degrees, an intermediate angle of 45 degrees was selected for the present investigation. Detailed turbulence data can be obtained with the specially constructed facility. The development of the flow and instrumentation system and initial data from the new facility are presented herein.

TABLE OF CONTENTS

LIST OF FIGURES

NOMENCLATURE

d	diameter of nozzle 2 inches for jet near field study 0.75 inches for oblique jet impingement study
D/Dt	material derivative
h	height of jet exit above the plate
L	distance of the jet exit from the geometric impact point of the jet centerline
p	static pressure
r	radius (r, θ, z coordinate system, see Figure 2)
u v w	velocity components in the r, θ, z or x, y, z coordinate directions
U	mean velocity for jet near field study
x, y, z	rectangular coordinates (see Figure 2)

Greek Symbols

α	incidence angle of jet
Γ_x	separation distance of longitudinal correlation function
θ	angle in r, θ, z coordinate system (see Figure 2)
λ	momentum flux correction factor (see Figure 30)
ν	kinematic viscosity
ρ	density

Special Symbols

$\overline{(\ )}$	time mean velocity
$(')$	fluctuating velocity
$\widetilde{(\ )}$	r.m.s. value
$\underset{\sim}{(\ )}$	vector quantity

1. INTRODUCTION

This communication is the third semi-annual progress report of the research supported by the National Aeronautics and Space Administration grant NGR 23-004-068. Its purpose is to indicate the status of the research program and the projected efforts which will be made during the duration of this year's activity.

Two, concurrent investigations are in progress. The oblique jet impingement work is being continued to provide mean surface pressure, mean velocity and turbulence intensity information for a characteristic large angle configuration (α = 45 degrees). Secondly, a comprehensive study of the exit plane turbulence structure influence on the near field of an axisymmetric jet is in progress. The scope of these two studies, the bases for them, and the necessary equipment and procedures along with some documentation and preliminary results are given herein.

The basic mechanics of the shallow angle, jet impingement flow field have been inferred from an extensive analysis of the surface pressure and mean velocity data for the range $3 \leq \alpha \leq 15$ and $0.5 \leq h/d \leq 2.0$. The flow model which integrates the identified mechanics into a comprehensive description is presented in [1]. This model can be briefly summarized as follows. The presence of the plate requires the jet to spread laterally or to deflect vertically. For sufficiently shallow angles, the primary response is an upward curvature with pronounced spreading only for angles above 15 degrees. The basic processes, and hence the structure of the model, are dependent upon the vorticity effects of the flow, specifically, (i) production by stretching and reorientation of the circular vortex loops of the approach jet and (ii) the flux of vorticity through the surface associated with the surface pressure gradients.

A new flow system has been constructed to allow quantitative data to be acquired for the large angle cases. A schematic of this unit is shown in Figure 1. It should be noted that a new coordinate system is adopted for these higher angle cases; viz., the origin is located at the intersection of the jet axis and the plate (see Figure 2) and the rectangular (x, y, z) and cylindrical (r, θ, z) coordinate systems are used as appropriate. A detailed description of this flow system is given in the "Experimental Equipment" section. Initial results have been

acquired and are included in this report.

The second major activity in the continuing studies is a comprehensive investigation of the effect of initial conditions upon the near field of an axisymmetric jet. Following the first year's efforts, it was recognized that the structure of the flow at the exit plane of the jet had a pronounced effect on the entrainment of mass in the near field region and an effect on the surface pressure distribution for the impingement flow field. Also, the mean velocity data, from several studies of the near field as reported in the literature, were used to define the mass flux as a function of the streamwise location. These results, shown in Figure 3, can be used to infer that the turbulence structure at the exit plane is primarily responsible for the behavior of the jet in the near field [1]. The importance of the initial condition effects on the behavior of the flow and the lack of any comprehensive study of these effects motivated this investigation. The analytical basis for the initial condition effects is presented in the next section.

The study of the initial condition effects will provide basic research support for another aspect of the National Aeronautics and Space Administration mission, namely, the development of quieter propulsion systems. The multitube shrouded nozzle for jet engines is a configuration which has been proposed to reduce the jet noise at a given thrust value. The multiple jets, which are formed and coalesce in a region bounded by an acoustic shroud, serve to reduce the total radiated sound power of the resultant jet. The complexity of this configuation means that a broadly based approach for its analysis and development is appropriate. Such an approach can involve studies ranging from acoustic measurements to the characteristics of the mean velocity field to the turbulence structure of the resulting jet. However, it is important that each of these investigations seeks to establish information which is both relevant to the application problem and instructive regarding the basic nature of the flow. Specifically, if one seeks to investigate the mechanics which control the turbulence structure (which in turn controls the acoustic emission) one must be careful to acquire data which do not simply reflect the particular device.

It is in this context that the investigation of the initial condition effects on the near field of an axisymmetric jet is considered a

contribution to the analysis of the multitube shrouded nozzle. At the end of the shroud, the multiple jets form an effective jet with a strongly disturbed character. The turbulence characteristics of this jet are quite different from those of a jet with a uniform mean velocity and quiescent* core flow ($\tilde{u}/\bar{u} << 1$ except for the annular shear layer region). The dominant noise producing region of a jet is recognized to be the near field ($0 \leq x/d \lesssim 10$) since this is the region of the greatest shear stress magnitudes which contribute to the quadrupole source terms identified by Lighthill [2, 3]. Consequently, the numerous studies of the noise producing region including those of Laurence [4], Ko and Davies [5], Davies, Fisher and Barratt [6], Bradshaw, Ferris and Johnson [7] and Maestrello and McDaid [8] are not directly applicable to the multitube jet. However, these investigations are of considerable value as reference cases for the disturbed jet results.

The initial condition effects will be studied in a systematic manner made possible by a unique technique wherein the scale and the intensity of the exit plane turbulence structure can be separately controlled while a uniform mean velocity profile is maintained. The purpose of this initial investigation is to establish the response of the jet to these control parameters for the region $0 \leq x/d \leq 10$. This is the first phase of a total investigation which will provide the equivalent and additional information for the disturbed exit plane condition as that provided by the above studies for the quiescent exit plane condition. The data to be acquired will be used to define $\bar{u}$, $\bar{v}$, $\tilde{u}$, $\tilde{v}$, $\overline{uv}$, and the same quantities conditionally sampled upon the presence or absence of vortical fluid at the probe location during the time period over which the statistical quantity is being formed. This requires a quite elaborate data acquisition system, appropriate analog signal processing and the use of the Texas Instruments mini-computer to process the digitized hot-wire signals. These details will be deferred until the final report when the results of this investigation will be presented.

It is pertinent to note that this experimental capability will allow the investigation of the basic flow structures that Laufer [9] has found

*Defined as a low value of the r.m.s. level of the turbulent fluctuations $\tilde{u} = [\overline{(u - \bar{u})^2}]^{1/2}$.

to be related to acoustic jet noise. That is, Laufer has found preliminary evidence that the acoustic noise characteristics are related to the coherent structures which exist in an apparently random spatial and temporal distribution in a turbulent flow. These coherent structures have only recently been observed in turbulence research with the advent of the conditional sample techniques pioneered at the Johns Hopkins University, Kovasznay, Kibbens, and Blackwelder [10], and at the University of Southern California, Gupta, Laufer, and Kaplan [11]. Their identification has been responsible for a considerable rejuvenation of interest in turbulence research and a marked increase in our knowledge regarding turbulent flows. The classical notions of acoustics and of turbulence have involved "long term" averages. The essential message derived from the conditional sample techniques is that such averages "smear over" the mechanistic processes which govern the motion; hence, the long term average, albeit "true," masks the information requisite for understanding.

This report will present the analytical basis for the specification of the initial conditions, the experimental apparatus to achieve the independent control over the scale and intensity of the turbulence while maintaining a (spatially) uniform mean velocity distribution, and the data to document the exit conditions.

2. ANALYTICAL BASIS FOR THE INITIAL CONDITION STUDY

The flow characteristics and turbulence structure in the near field* of an axisymmetric jet are influenced by the conditions at the exit plane of the nozzle. Flow characteristics and turbulence structure are herein defined to include such measures as the mean velocity field, the turbulence intensity and Reynolds shear stress distributions, the entrainment of the surrounding fluid (i.e, the transmission of vorticity to previously non-vortical ambient fluid) and the transport of mixing of scalar contaminants such as thermal energy. These quantities are susceptible to experimental evaluation and, for some of the measures,

*The term "near field" is used to denote the region in the jet flow from the exit plane to a position sufficiently far downstream that the jet has nearly attained a "self-preserving" character.

to analytical calculation given appropriate closure models. It is the purpose of this section to identify the analytical basis for the effect of the initial conditions.

The influence of the initial conditions on the development of the axisymmetric jet can be expressed by considering the mathematical description of the problem. The Navier-Stokes equations are considered to be the applicable dynamic equations for the instantaneous motion. (The motion is considered to be that of an incompressible fluid such that the dynamic equations provide a sufficient description.) The instantaneous motion presents a formidable mathematical problem not only because of the non-linear character (as in the laminar motion), but also because of the unsteady character of the motion. Experimentally, the time dependence of the motion would imply that a complete field description would necessitate simultaneous measurements secured at a rapid rate from "all" parts of the flow. Fortunately, the instantaneous information is not required for many engineering purposes and stochastic averages are satisfactory. That is, the ergodic theorem is invoked (time averages identically equal to ensemble averages) and average velocities, turbulent intensities, and multi-point, multi-velocity correlations are introduced into our description of the motion.

This review of the averaging process, so commonly used in turbulence work, deals with well known concepts; however, it is required to adequately describe the nature of the current study. Specifically, the mathematical problem under consideration involves the time averaged equations for the mean velocity (1), the Reynolds stress or velocity covariance (2), and the other second and higher order equations which will not be written.

$$\frac{D\bar{U}_i}{Dt} = -\frac{1}{\rho}\frac{\partial p}{\partial x_i} + \nu\frac{\partial^2 \bar{U}_i}{\partial x_j \partial x_j} - \frac{\partial}{\partial x_j}\,\overline{\dot{u}_i \dot{u}_j} \qquad (1) \quad (2.4.8 \text{ from } [12])$$

$$\frac{D\overline{\dot{u}_i \dot{u}_j}}{Dt} = -\left(\overline{\dot{u}_i \dot{u}_\ell}\,\frac{\partial \bar{U}_j}{\partial x_\ell} + \overline{\dot{u}_j \dot{u}_\ell}\,\frac{\partial \bar{U}_i}{\partial x_\ell}\right) - \frac{\partial}{\partial x_\ell}\,\overline{\dot{u}_i \dot{u}_j \dot{u}_\ell}$$

$$-\frac{1}{\rho}\left[\overline{\dot{u}_i \frac{\partial \dot{p}}{\partial x_j}} + \overline{\dot{u}_j \frac{\partial \dot{p}}{\partial x_i}}\right] + \nu\left[\overline{\dot{u}_i \frac{\partial^2}{\partial x_\ell^2}\dot{u}_j} + \overline{\dot{u}_j \frac{\partial}{\partial x_\ell^2}\dot{u}_i}\right]$$

(2) (2.4.9 from [12])

These equations involve at least first-order terms with respect to the streamwise direction, x, (assuming a boundary layer like behavior, i.e., a narrow flow field) and these terms require initial conditions. The extraction of the necessary and sufficient boundary conditions for these stochastic equations is somewhat difficult to perceive. A simpler approach is to reconsider the original Navier-Stokes equations to identify the appropriate boundary and initial conditions considering the equations to be at most first-order in x. The complete solution for the velocity field $u_i(\underline{x};t)$ requires at least a description of the velocity over the exit plane at an instant, i.e., $u_i(0, y, z;0)$. The stochastic equations remove the initial condition dependence in favor of averaged values of the velocity and, without proof, this is assumed to be the equivalent of specifying averaged functions of the velocity. Specifically, the velocity field averaged at a point would introduce such quantities as $\overline{U}_i(\underline{x})$, $\overline{\dot{u}_i \dot{u}_j}(\underline{x})$, $\overline{\dot{u}_i \dot{u}_j \dot{u}_k}(\underline{x})$ ... as might be expected intuitively. It also requires such averages as $\overline{\dot{u}_i(\underline{x})\, \dot{u}_j(\underline{x} + \underline{r})}$, $\overline{\dot{u}_i(\underline{x})\, \dot{u}_j(\underline{x} + \underline{r})\, \dot{u}_k(\underline{x} + \underline{r} + \underline{s})}$, ... , that is, the measures which contain the information regarding the scale of the motion. Clearly, an infinity of such measures could be considered both sufficient and totally unrealistic in terms of meeting the physical science objectives of describing such a flow field or the engineering objective of calculating its behavior. It is not obvious what stochastic measures of the initial conditions are necessary and sufficient for either of these two purposes.

The experimental research program proposed herein will examine the effect of systematically controlled initial conditions on the flow development in the near field of an axisymmetric jet. The arguments based upon the instantaneous and averaged Navier-Stokes and higher-order equations resulted in the observation that an infinity of stochastic conditions is sufficient for the specification of the boundary conditions. The proposed study is based upon the hypothesis that the turbulence structure interior to the (thin) shear layers at the exit plane of the nozzle is the important, if not the dominant, physical aspect of the initial conditions. It is further hypothesized that this turbulence structure can be satisfactorally characterized by separate measures of the intensity and scale. The technique to independently control these quantities and the documentation of the conditions at the exit plane of the jet are described separately in later sections.

3. EXPERIMENTAL FACILITY

3.1. The Study of the Initial Condition Effects

3.1.1. Flow facility

A large centrifugal fan (speed control to ± one percent) with an induced flow 7.5 in. pipe test section and a large plenum chamber on the pressure side is available for this work (see Figure 4). The 105 diameter long pipe is used to evaluate the performance of the hot wire data acquisition system by comparison with the universal fully-developed pipe flow results of Laufer [13] and by the absolute evaluation of the Reynolds stress term ($-\rho \overline{\tilde{u}\,\tilde{v}}$) from its linear variation with respect to radius and its magnitude as determined from the pressure gradient in the pipe. Such a procedure is used to determine the precise (and operationally defined) angle between the two wires of an x-wire array. Such an evaluation scheme is described by Patel [14]. The plenum chamber has been modified to accommodate the jet flow apparatus for the present study. The air from the plenum chamber is accelerated through the contraction into the 3 in. tube shown in Figure 5. The array of jet tubes at the inlet section is connected via pressure regulators and an air cleaner, to the building air supply. The jet tubes are 0.043 in. internal diameter and grids of 0.3, 0.4 and 0.5 in. spacing are available. The small plenum at the exit of the 3 in. tube is evacuated by an auxiliary blower such that the dividing stream surface is positioned at or inside the knife edge on the 2 in. long, 2 in. diameter tube. Consequently, the exit plane flow is a combination of the quiescent plenum flow mixed with the flow from the jet tubes in a ratio determined by the jet tube air supply pressure. Data on the condition of the flow at the exit plane will be presented in the "Results" Section. The jet exhausts from a plane wall fitted with static taps located along a radial line from the nozzle edge to a distance of 8 diameters.

3.1.2. Data acquisition and processing facility

3.1.2.1. Transducers

Four channels of linearized, constant temperature hot-wire anemometers are available for this study. As discussed below, the linearizers are utilized as signal conditioners since a calibration technique is used to relate the voltage output to the velocity in 0.25 fps

intervals. Model 308 Decker capacitive pressure transducers are available for the required pressure measurements. The voltage-velocity calibration of the hot-wire anemometers makes use of these transducers. These units provide a linear 0-10 volt output for 0 - 3 inches of water (differential pressure).

3.1.2.2. Data acquisition

A Texas Instruments mini-computer (Model 960A) with a 16K memory is available for the on-line acquisition and initial processing of the experimental data. The cycle and arithmetic operations time of this machine are sufficiently fast that the data acquisition schemes are based upon: (1) reading a sample from the digitized transducer output (20 khz A-D Converter), (2) using this sample to update the statistical quantities desired in the data run, (3) returning and securing another sample. The statistical quantities of interest are the mean, standard deviation, (possibly skewness and flatness), auto correlations and cross correlations with or without time delay. The use of the digital techniques allows this data processing to be executed with the velocity rather than the transducer voltage values since it is possible to convert the latter between steps 1 and 2 above. This eliminates the errors associated with "linearizing" the response equations and is especially effective in the relatively low frequency, large fluctuation region at the edge of the jet. Conversely, the high frequency, i.e., dissipation, information involves relatively small amplitude variations such that a rapid read and process technique would be effective. For these data, the voltage magnitudes will be used and the statistical values will be converted. A major advantage over the analog signal processing (in addition to computing with the velocity, not voltage, values) is that of the crest factor limitation of conventional r.m.s. voltmeters and the formation of long term averages via digital as opposed to integrating analog devices. The latter are either expensive or suffer from drift problems or both.

The major advantage of the digital acquisition system is its capability to perform conditional sample statistics under soft-ware, not hard-ware control. This capability will be primarily used for the studies of the basic mechanics of the turbulent motion and the entrainment.

The "up-dated average" technique described above is the only possible scheme to employ given the size of the core memory available.

Considering the soft-ware requirements for the sample and calculate routines, only a relatively few positions from the flow field can be sampled before the core is filled. The laboratory is connected by cable to the IBM-1800 computer located in and available to the College of Engineering. This unit has card read/punch, line printer and disc storage peripherals. The disc storage is available in such a manner that data processing programs and processed data can be stored and be available on a time share basis with other users. A schematic of the transducers, computers and traverse device is presented in Figure 6.

3.1.2.3. Traverse and control systems

The traverse device to position the probe is mounted on a rigid support (lathe bed and tool holder). Stepping motors drive the various gear trains to position the probe in x-y-z-θ (θ is the angle of the probe shaft in the x-y plane). Tolerance values of x = $\pm$0.01, y = $\pm$0.001 and z = $\pm$0.001 inches and θ = $\pm$0.1 degrees are made possible by the rigid support and fine position drive components. The control signals for the stepping motors can be generated by manual or computer control. Under computer control, a traverse, e.g., radial, r, at an angle $\tan^{-1} z/y = \pi/6$, can be programmed for the desired number of steps of a given size (e.g., 0.1 in.); the desired statistical averages and the data will be recorded and processed automatically. This capability has proved quite useful in terms of executing simultaneous readings from two x-wires and orienting the probe until the shaft is aligned with the mean flow direction. Since this is the direction for which the probe is calibrated, the readings will be made with maximum accuracy.

3.1.3. Data processing

The hot-wire and pressure transducer voltages are digitized via an A-D converter on either the Texas Instruments 960A or IBM 1800 computer. The maximum sampling rate of these 16 bit converters is 20 and 10 khz, respectively. This is satisfactorily above the Nyquist rate for the highest frequencies expected in the flow to be investigated and the calibration procedure respectively as per their use.

The hot-wire response is calibrated by use of a pitot tube in a quiescent jet stream. Depending on the requirements for the available

core memory and the required speed of the conversion for the data readings, either a calibration table listing the velocity as a function of voltage for 0.25 fps intervals or a fourth-order curve is used as the calibration reference data.

The computation of the mean, standard deviations, etc. is relatively straightforward using the "updated average" technique presented earlier. It should be noted that the schemes to compute the various statistical quantities are selected to be compatible with the nature of the frequency content and amplitude variation of the values.

3.2. The Large Angle Jet Impingement Study

3.2.1. Flow facility

The larger angles of current interest have necessitated that an entirely new flow system be constructed. The shallow angle cases required only that velocity data be acquired in a plane transverse to the mean flow direction; such a direction was well defined along the axis of the jet. The larger angle cases will involve a velocity field that is distributed over 360 degrees; hence, provision must be made to measure over this range. The new flow system is shown schematically in Figure 1. This unit has the features that (i) the distance from the jet exit to the plate is continuously adjustable over a large range $0 \leq L/d \lesssim 20$; (ii) traverses may be obtained at 15 degree increments from $0 \leq \theta \leq 180$ degrees; and (iii) the angle α is altered only by the utilization of a support plate of a different angle ($\alpha = 45$ degrees presently). A single row of static taps allows the acquisition of mean surface static pressure data. The end plate is curved to allow the probe to be oriented at the angle of the flow (this eliminates yaw errors) and to be traversed along a line perpendicular to the lathe bed.

3.2.2. Data acquisition and processing facility

The material of the preceeding and equivalent subsections applies equally to this investigation. It should be further noted that the traverse device will always be moved along the same line above the plate although the equivalent θ value will change as the jet support is rotated. The probe will be aligned with the direction of the flow by the on-line computer controlled stepping motors. An appropriate algorithm aligns the probe into the flow.

4. RESULTS

4.1. Presentation and Interpretation of the Documentation Data for the Flow at the Exit Plane

4.1.1. Presentation

Mean velocity, turbulence intensity of the streamwise velocity, and the scale of the turbulent motions as revealed by the auto correlation of the streamwise velocity fluctuation were recorded at multiple locations over the exit plane of the previously described jet. These data are presented in Figures 7 to 14 for the mean velocity and the relative intensity and in Figures 15 to 22* for the normalized auto correlation functions. The former are from a diametral traverse across the jet exit, similar data were observed at equivalent radial locations. The auto correlation values have been converted to a function whose argument is the separation distance. The original data were time correlations from a P. A. R. 101 correlation function computer; the transformation was made by application of the Taylor hypothesis ($\delta r = U\delta\tau$). The sampling points are shown by locating the same symbol on the nozzle exit plane as is used to denote the autocorrelation values. The auto-correlations in the shear layer show distributions in which substantially more energy exists in the small scales; this reflects the active production and dissipation of these regions. The turbulence structure in these shear regions will be recorded for the conditions investigated; however, no attempt to control this structure will be exercised.

The average values for the auto correlation functions have been computed for a given set of control conditions (grid size, pressure level, fan rpm). These averaged data may be used for comparisons of the results for various control conditions; such comparisons are shown by Figures 23 to 29*. Figures 23 to 25 show that essentially the same scale for different intensities can be achieved by using different mesh sizes, a constant blower speed, and a constant supply pressure for the pressure tubes. Figures 26 to 28 demonstrate that for a given grid size, the variation of the supply pressure alters both the intensity and

*The abscissa for Figures 15 to 29 is shifted, the first point plotted is $\Gamma_x = 0$ instead of the 0.0125 in. value indicated.

the scale. Figure 29 presents a comparison of the autocorrelation functions for two cases which have nearly the same intensity. It is possible to easily create other situations of equivalent intensity with different scales by proper adjustment of the pressure level. Note that the non-homogeneities in U are of the order 1-2 percent except for the zero blower RPM cases. The non-homogeneities in the $\tilde{u}$ values are nominally 10 percent with the exception of the 0.3, 15, 0 case.

4.1.2. Interpretation

An interpretation of these results indicates that the scale is more strongly controlled by the effective transit time required for the flow to travel the length of the 3 in. conduit (i.e., from the exit of the jet tubes to the exit plane of the jet) rather than by the spacing of the grid. This implies that an alternate control on the intensity level for a given scale can be achieved by the distance from the jet tubes to the exit plane of the jet. The effect of this parameter has been investigated; unfortunately, it is not possible to obtain larger intensities and to maintain a streamwise homogeneous condition.

4.2. Velocity, Turbulence Intensity and Surface Static Pressure for a Large Angle Oblique Jet Impingement Case

4.2.1. Presentation

A nominal quantity of data is presented in this report to demonstrate the nature of the acquisition scheme and to present preliminary results for the α = 45 degree condition. An h/d = 1.5 (or L/d = 2.12) case is reported herein.

Surface pressure data are presented in Figure 30 in the form of normalized isobar contours. The indicated pattern is to be expected based upon the α = 30 and 60 degree cases presented in [1].

Both horizontal and vertical traverses to record the mean velocity and the turbulence intensity were acquired for the indicated geometric conditions. These are presented in Figures 31 to 34 for the horizontal traverse and in Figure 35 for the vertical. The horizontal traverse data have been normalized using the velocity calculated from the plenum velocity, i.e., the inviscid flow velocity which is expected over the bulk of the exit plane (an exit plane traverse has not yet been recorded). The vertical traverses are normalized upon the maximum velocity in

the traverse; it is felt that this allows for optimal comparison between the various sets of data. Figure 36 presents a comparison of these horizontal traverse data.

4.2.2. Interpretation

The comparison plot of the horizontal traverse data shows that the vertical gradients are quite small over an extensive portion of the streamwise direction in the region near the plate surface. The r/d = 1 and 3 vertical traverse data (see Figure 35) show the domain of the small vertical gradient. The implied velocity gradient at the plate surface is quite large since the velocity falls to zero within a span of about 0.01 in. from the indicated maximum value. The relatively constant turbulent intensity values are apparently the result of a strong lateral diffusion by the turbulence, i.e., a $\partial \overline{\dot{u}^2 \dot{w}}/\partial z$ effect, since the dominant production term $-\overline{\dot{u}\dot{w}}\ \partial \bar{u}/\partial z$ is not large. Some production might be expected from the $\overline{\dot{u}^2}\ \partial \bar{u}/\partial x$ term although this contribution will not be significant at the r/d = 3 location. These results indicate that a significant portion of the flow is strongly disturbed (absolute intensity level $\tilde{u}/u_p \cong 0.2$). It would be interesting to observe the details of the flow quite near the surface; however, a larger nozzle would be quite desirable to obtain these data since the wire is vulnerable to breakage at physical distances less than the 0.01 in. setting used for the present results. Figure 36 presents a comparison of the two vertical traverses which demonstrates the decrease in the longitudinal velocity as a function of r/d.

5. REFERENCES

1. Foss, J.F. and S.J. Kleis, "The oblique impingement of an axisymmetric jet," Second Annual Report, Grant NGR 23-004-068, Michigan State University (December 21, 1972).

2. Lighthill, M.J., "On sound generated aerodynamically," Proc. Royal Society, A 211, 564-587 (1952).

3. Lighthill, M.J., "On sound generated aerodynamically, II. Turbulence as a source of sound," Proc. Royal Society, A 222, 1-32 (1954).

4. Laurence, J.C., "Intensity, scale and spectra of turbulence in mixing region of free subsonic jet," NACA Report 1292, (1956).

5. Ko, N.W.M. and P.O.A.L. Davies, "The near field within the potential cone of subsonic cold jets," J. Fluid Mech. 50, 1, 49-78 (1971).

6. Davies, P.O.A.L., M.J. Fisher and M.J. Barratt, "The characteristics of the turbulence in the mixing zone of an axisymmetric jet," J. Fluid Mech. 15 (1963).

7. Bradshaw, P., D.H. Ferris and R.F. Johnson, "Turbulence in the noise producing region of a circular jet," J. Fluid Mech. 19, 591-624 (1964).

8. Maestrello, L. and E. McDaid, "Acoustic characteristics of a high-subsonic jet," AIAA J. 9, 6 (1971).

9. Laufer, J., R.E. Kaplan and W.T. Chu, "Acoustic modeling of the jet noise abatement problem," Interagency Symposium on University Research in Transportation, p. 86, (March 28, 1973).

10. Kovasznay, L.S.G., V. Kibbens, and R.F. Blackwelder, "Large scale motion in the intermittent region of a turbulent boundary layer," J. Fluid Mech. 41, 2, 283-325 (1970).

11. Gupta, A.K., J. Laufer and R.E. Kaplan, "Spatial structure in the viscous sublayer," J. Fluid Mech. 50, 493 (1971).

12. Townsend, A.A., The Structure of Turbulent Shear Flows, (Cambridge University Press, 1956).

13. Laufer, J., "The structure of turbulence in fully developed pipe flow," NACA Report No. 1174 (1954).

14. Patel, R.P., "Measurement of the Reynolds stresses in a circular pipe as a means of testing a Disa constant-temperature hot-wire anemometer," McGill University Technical Note 63-6.

15. Alexander, L.G., T. Baron and E.W. Comings, "Transport of momentum, mass and heat in turbulent jets," University of Illinois, Engineering Experiment Station, Bulletin 413 (1953).

16. Sami, S., T. Carmody and H. Rouse, "Jet diffusion in the region of flow establishment," J. Fluid Mech. 27, 231 (1967).

17. Mons, R.F. and P.M. Sforza, "Turbulent heat and mass transfer in axisymmetric jets," PIBAL Report No. 71-14 (May 1971).

18. Crow, S. and F.H. Champagne, "Orderly structure in jet turbulence," BSRL Document D1-82-0091 (July 1970).

19. Hill, B.J., "Measurement of local entrainment rate in the initial region of axisymmetric turbulent air jets," J. Fluid Mech. 11, 1, 21-32 (August 1961).

20. Foss, J.F. and S.J. Kleis, "A study of the round-jet/plate-wall flow field," First Annual Report, Grant NGR 23-004-068, Michigan State University (October 8, 1971).

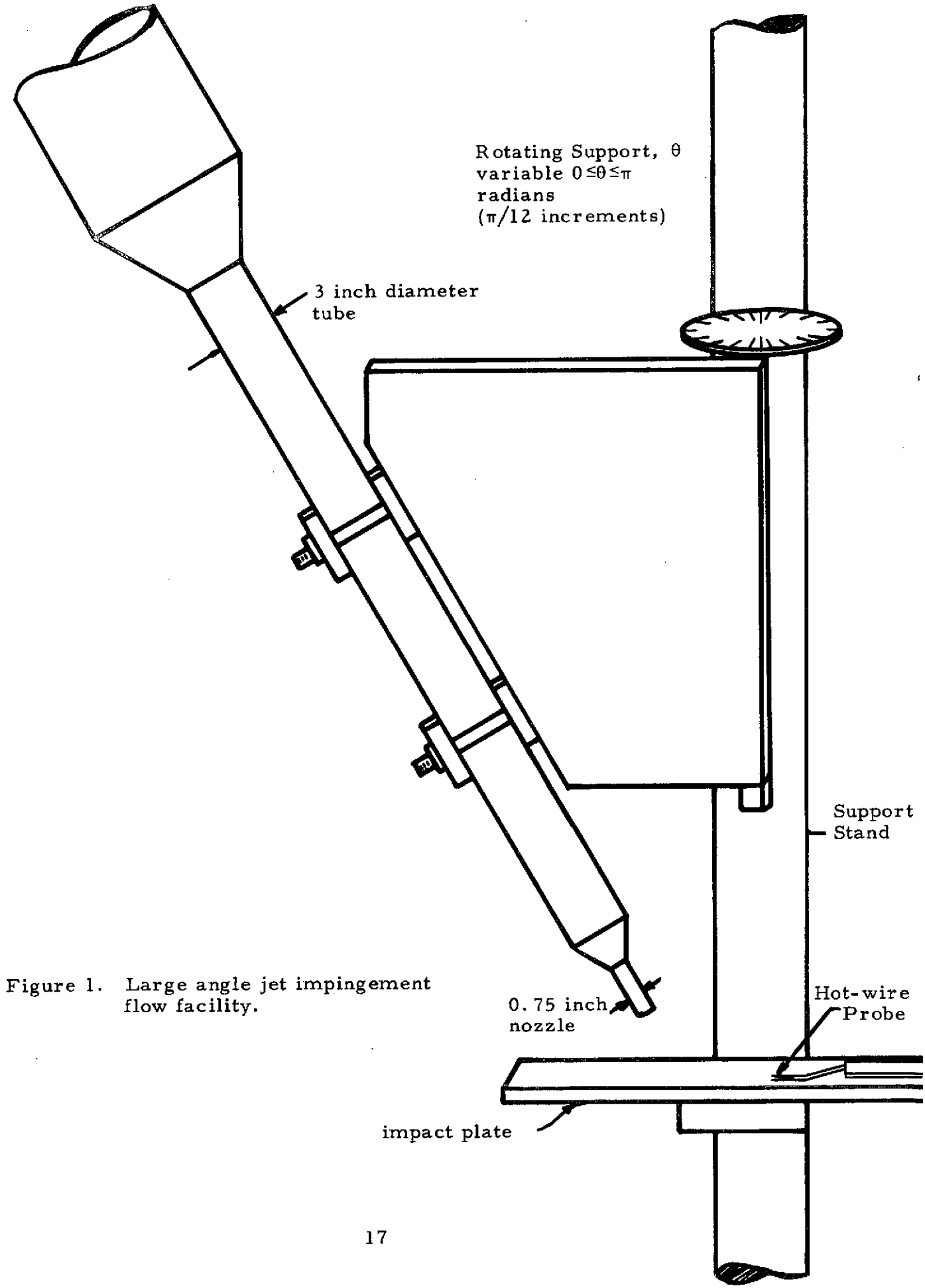

Figure 1. Large angle jet impingement flow facility.

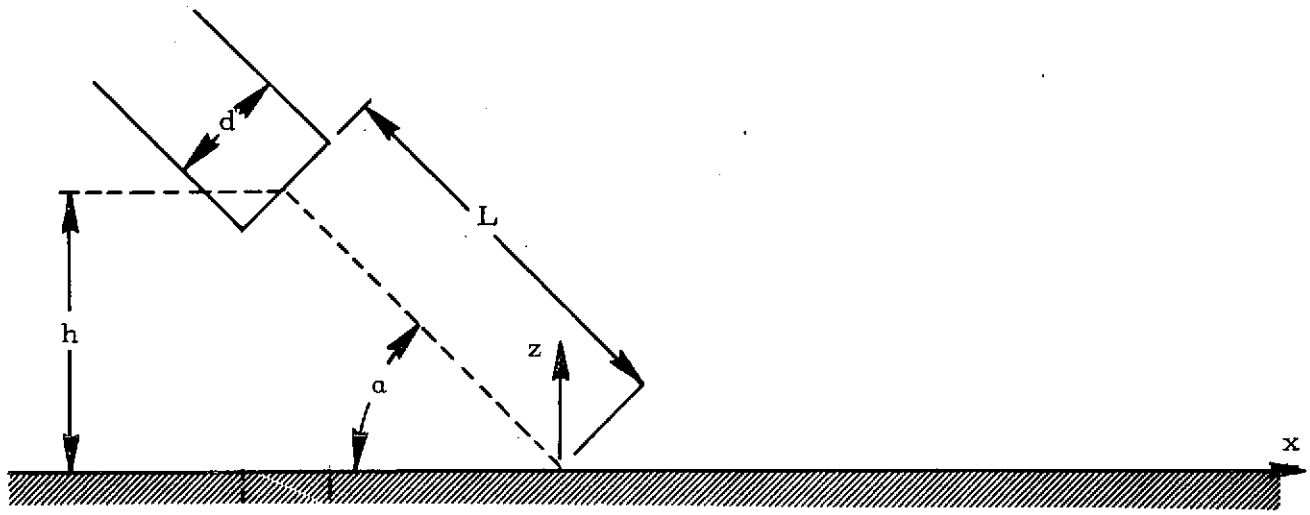

a. Side View

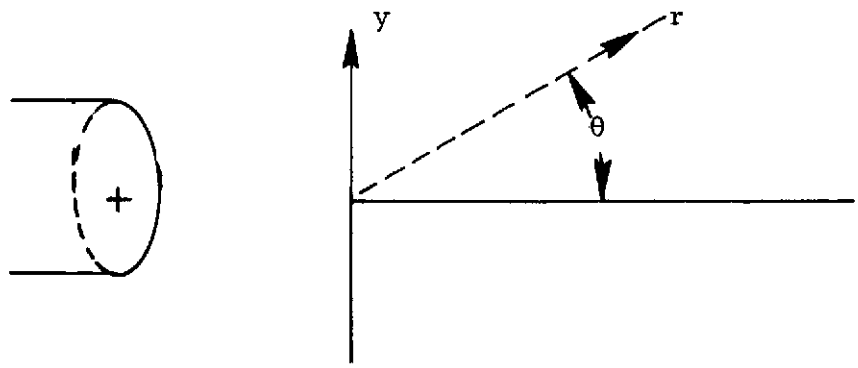

b. Top View

Figure 2. Coordinate system and definition of symbols for the large angle jet impingement studies.

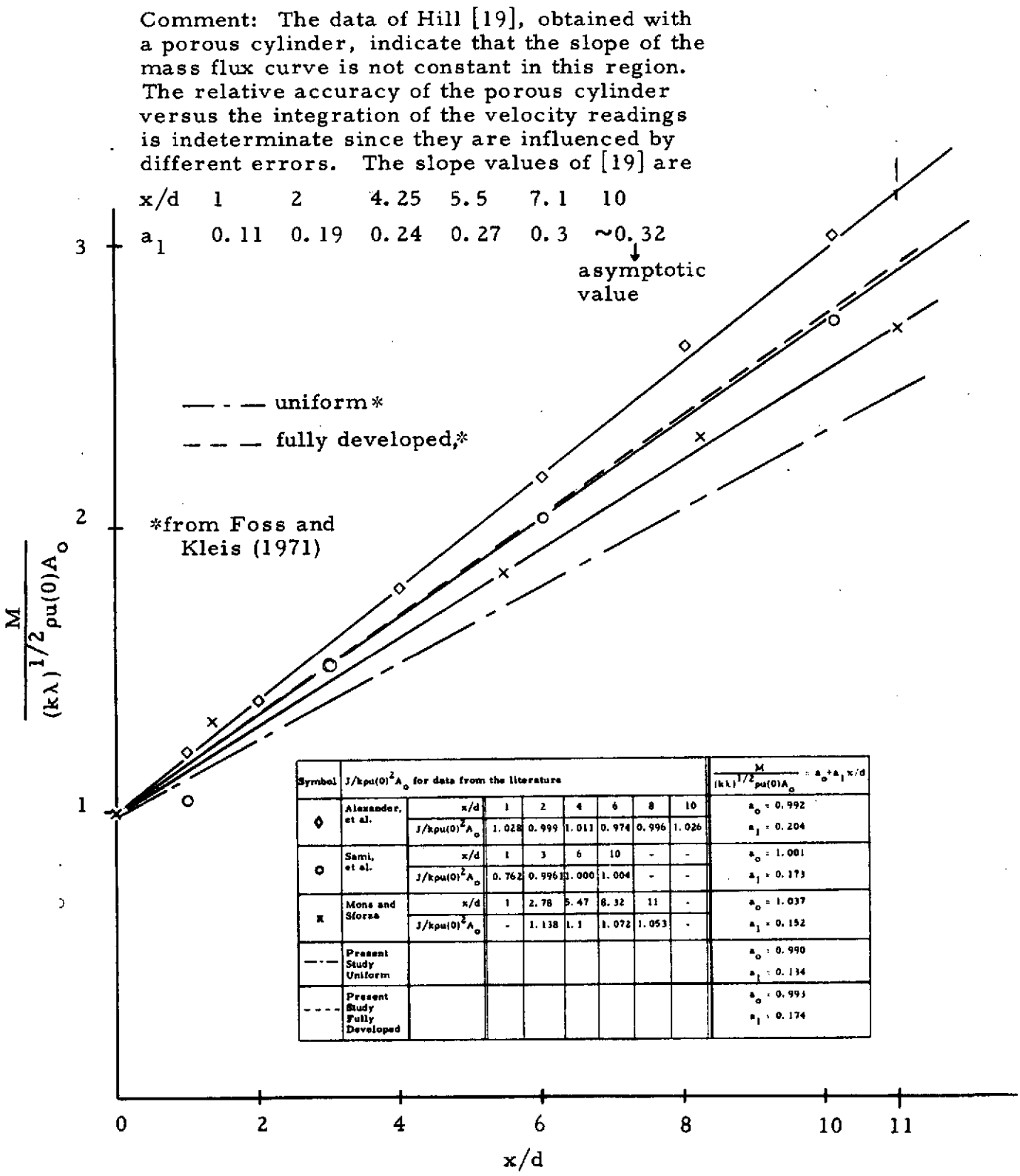

Figure 3. Normalized mass flux values as evaluated from references [15], [16], and [17] (data for Crow and Champagne [18] not shown, $a_1 = 0.136$ for $0 \le x/d \le 2$; $a_1 = 0.292$ for $x/d > 6$ of the present reference [20]).

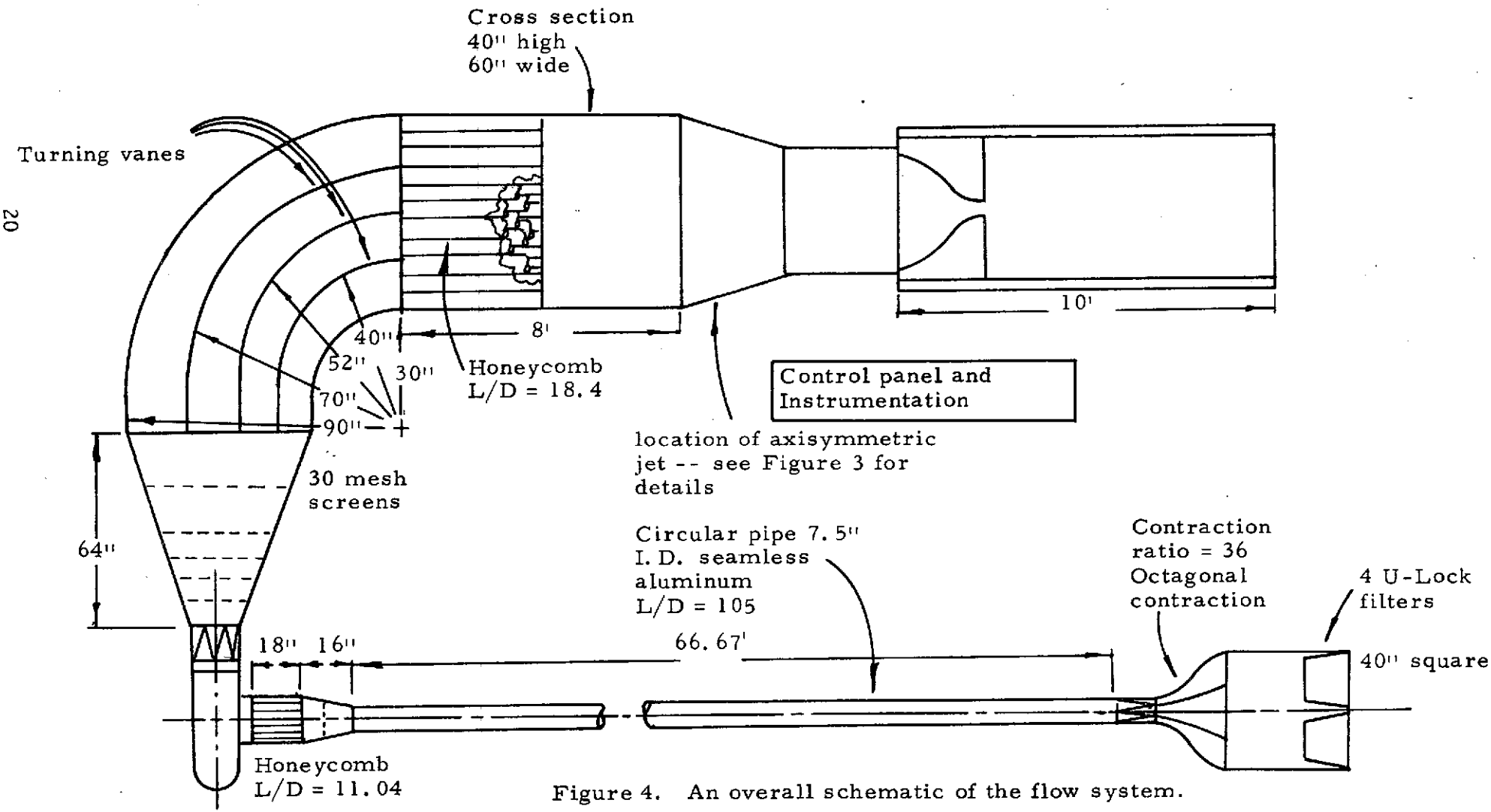

Figure 4. An overall schematic of the flow system.

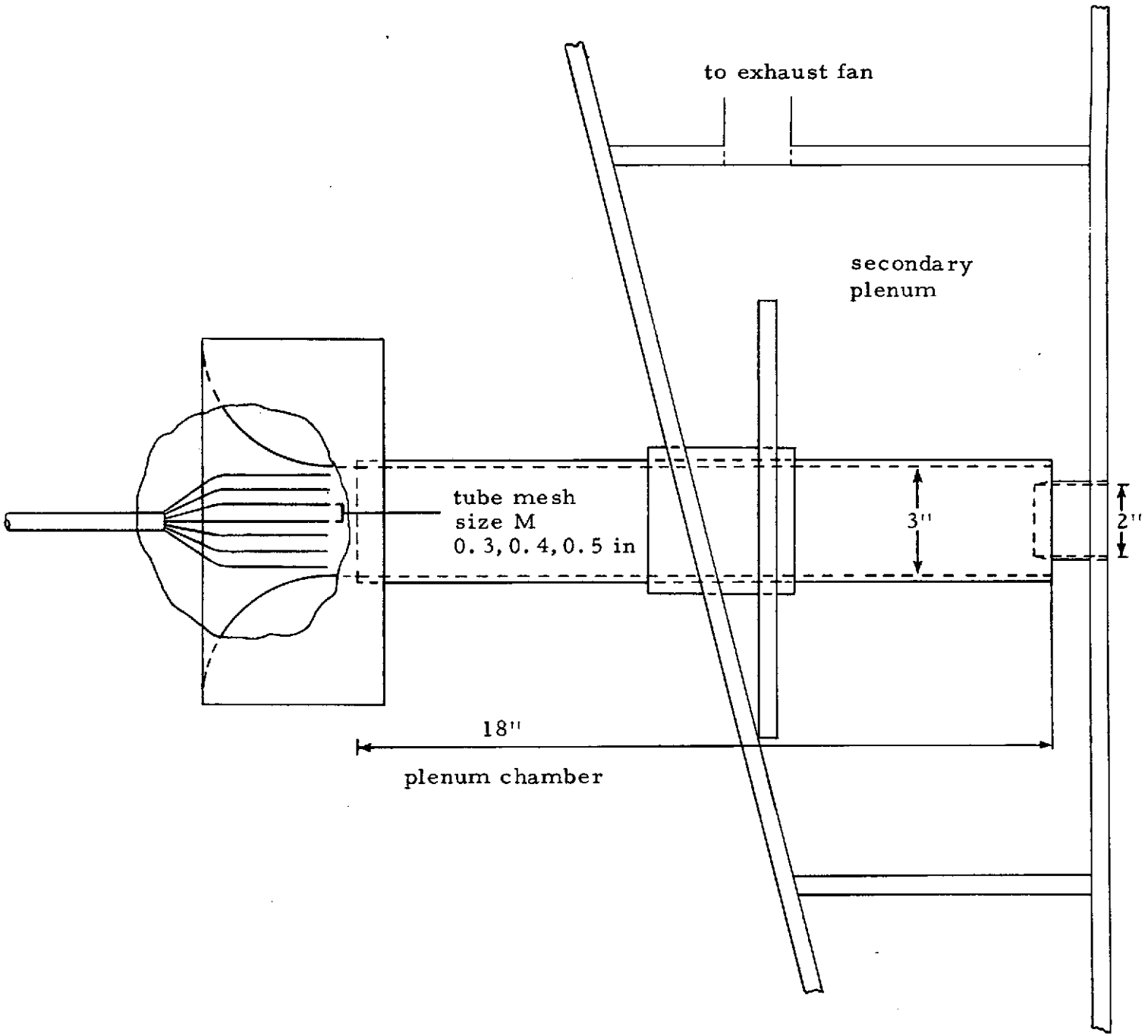

Figure 5. Configuration to achieve controlled intensity and scale at exit plane of axisymmetric jet.

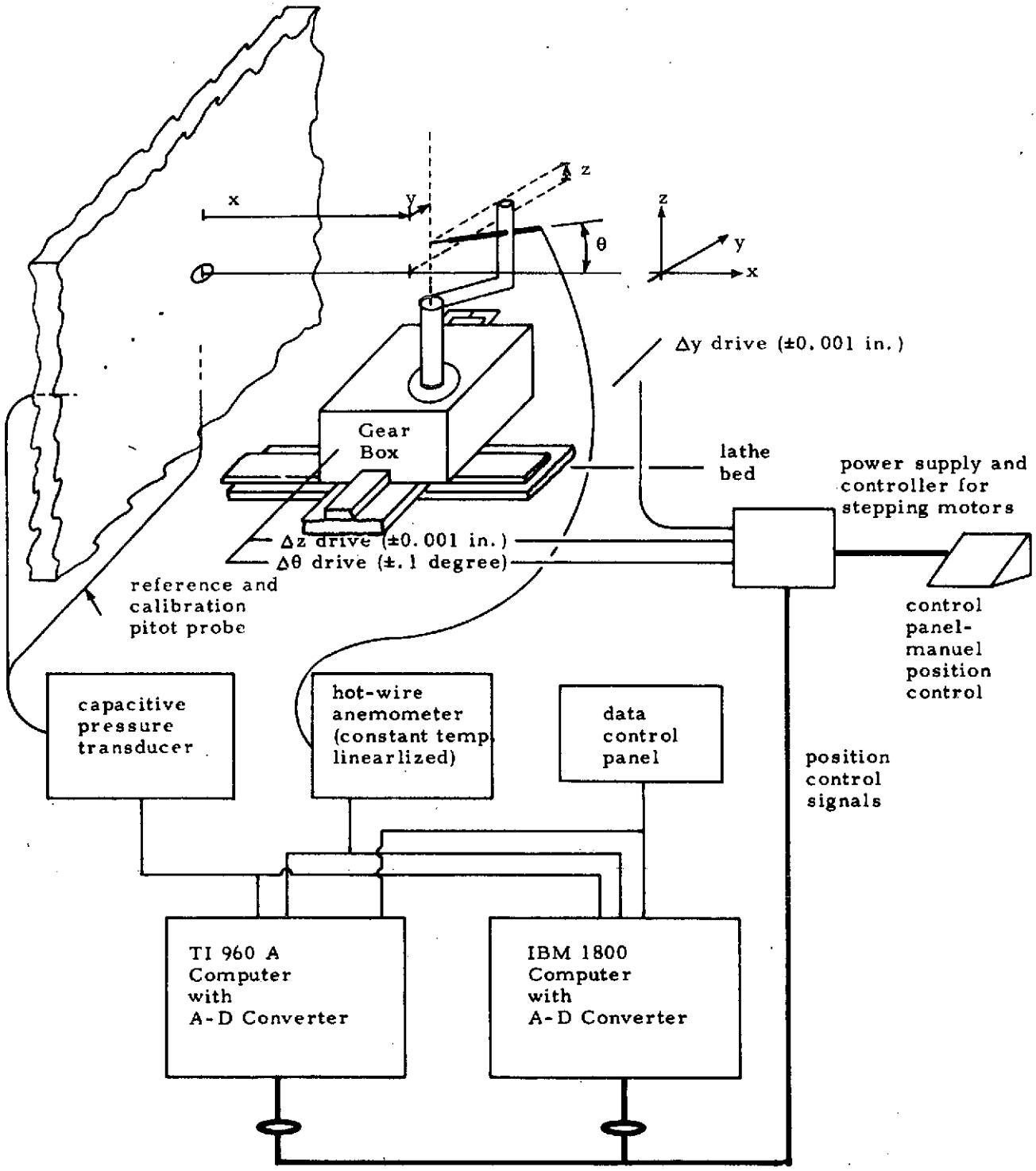

Figure 6. Schematic of data acquisition facility.

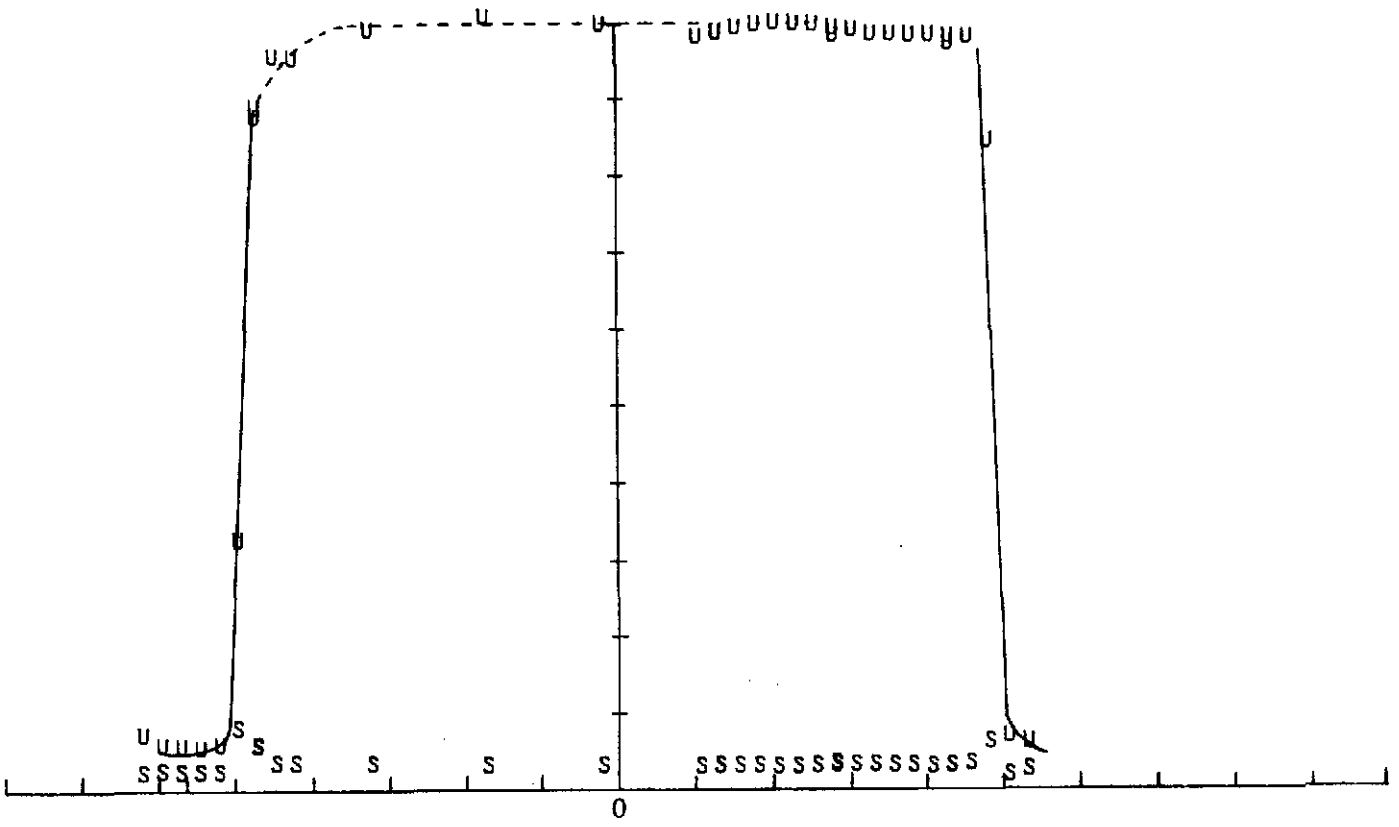

Figure 7. Mean velocity ratio, $U(0, y, 0)/\underline{U}(0, 0, 0)$, and the relative intensity of the longitudinal fluctuation, $u(0, y, 0)$ for the conditions 0.5, 15, 980. (Condition code: 0.5 = mesh size inches, 15 = pressure of jet tubes supply, 980 Blower Speed)

Note: Nominal mean velocity and r.m.s. relative intensity values are $U = 110.5 \pm 1.5$ fps and $\tilde{u} = 2.35 \pm 1.5$ percent. The tolerance values indicate the maximum deviations observed over the core region at the exit plane.

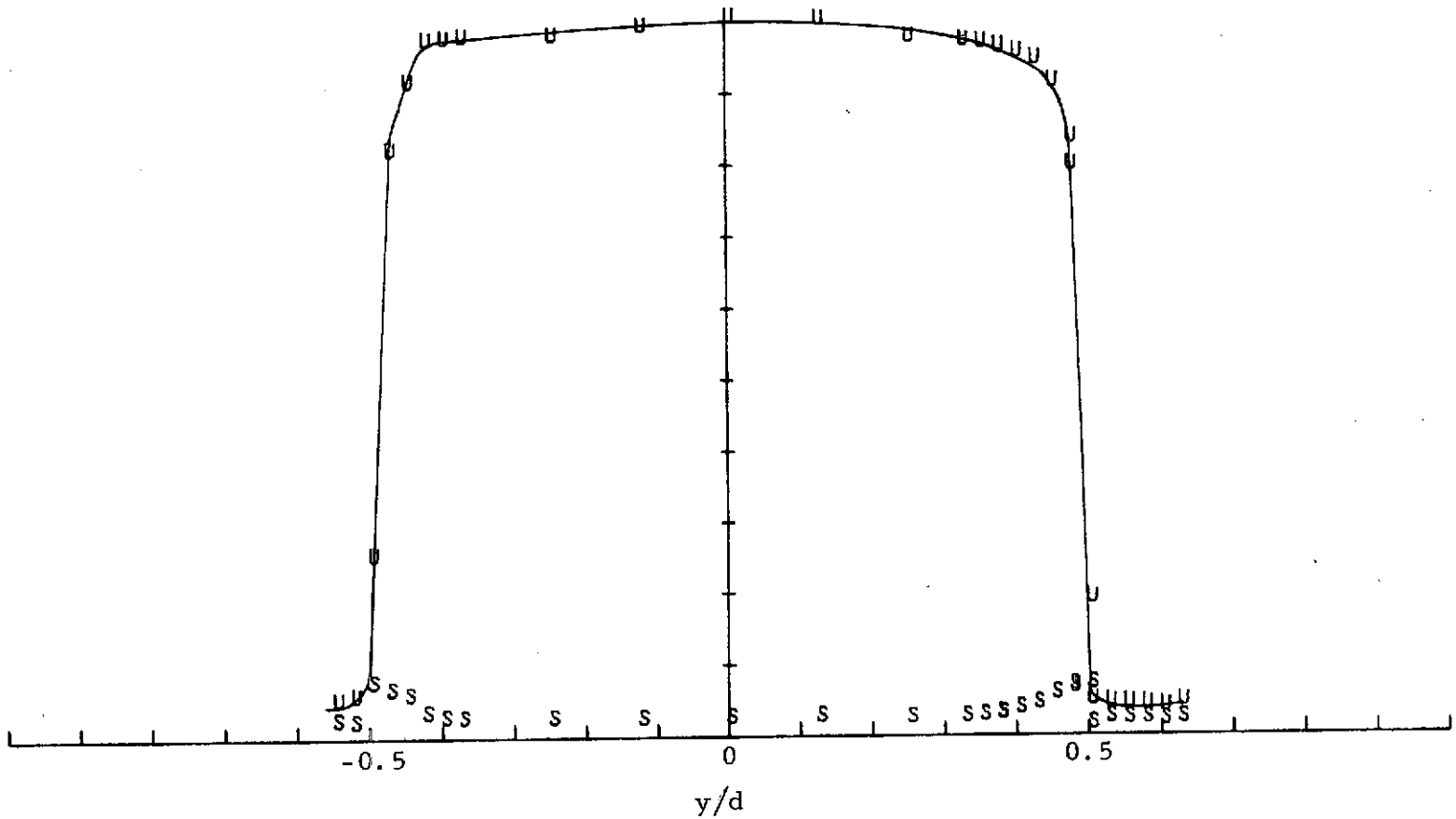

Figure 8. Mean velocity ratio, $U(0, y, 0)/U(0, 0, 0)$, and the relative intensity of the longitudinal fluctuation, $\tilde{u}(0, y, 0)$ for the conditions 0.4, 15, 930.

Note: Nominal mean velocity and r. m. s. relative intensity values are $U = 107 \pm 2$ fps and $\tilde{u} = 2.0 \pm 0.1$ percent. The tolerance values indicate the maximum deviations observed over the core region at the exit plane.

Comment: Misalignment of the jet tube array was apparently responsible for relative small core region. The resulting 3 inch tube boundary layer was responsible for the rounded mean velocity and increased $\tilde{u}$ values near edge of jet. This problem has been rectified.

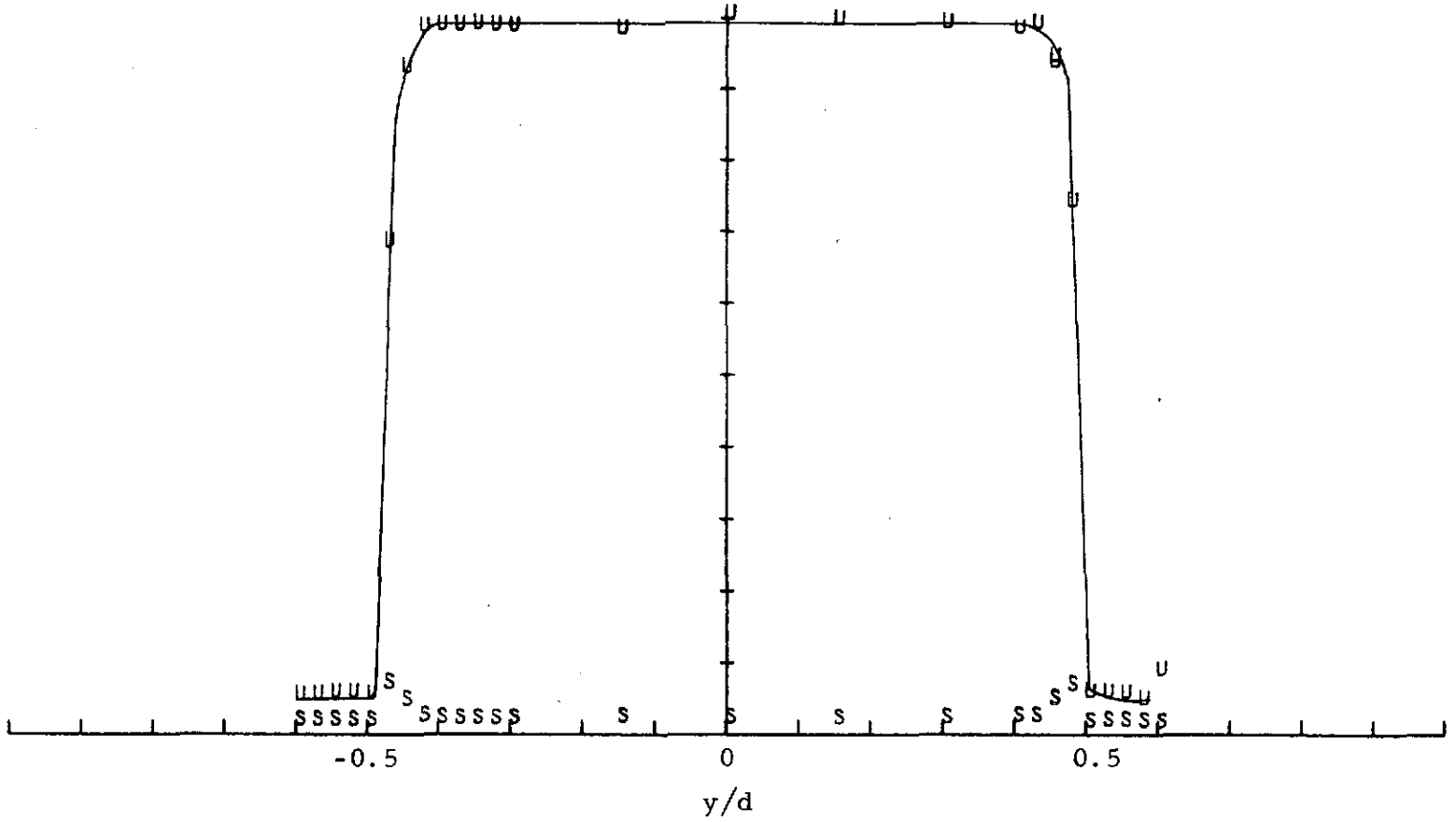

Figure 9. Mean velocity ratio, $U(0, y, 0)/U(0, 0, 0)$ and the relative intensity of the longitudinal fluctuation, $u(0, y, 0)$ for the conditions 0.3, 15, 980.

Note: Nominal mean velocity and r.m.s. relative intensity values are $U = 116 \pm 1.5$ fps and $\tilde{u} = 1.5 \pm 0.1$ percent. The tolerance values indicate the maximum deviations observed over the core region at the exit plane.

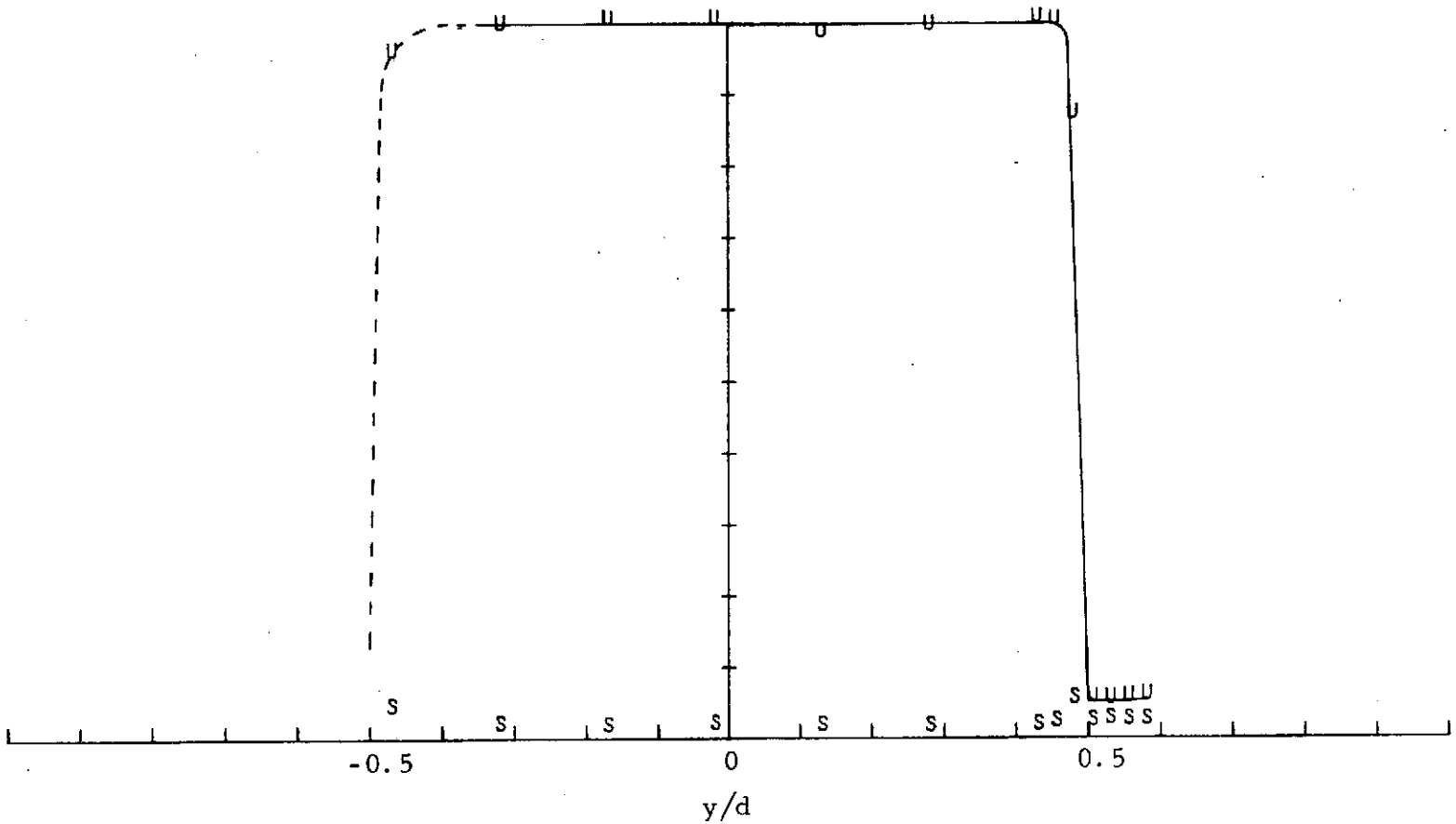

Figure 10. Mean velocity ratio, $U(0, y, 0)/U(0, 0, 0)$, and the relative intensity of the longitudinal fluctuation, $\tilde{u}(0, y, 0)$ for the conditions 0.5, 5, 980.

Note: Nominal mean velocity and r. m. s. relative intensity values are $U = 99.5 \pm 0.5$ fps and $\tilde{u} = 1.2 \pm 0.2$ percent. The tolerance values indicate the maximum deviations observed over the core region at the exit plane.

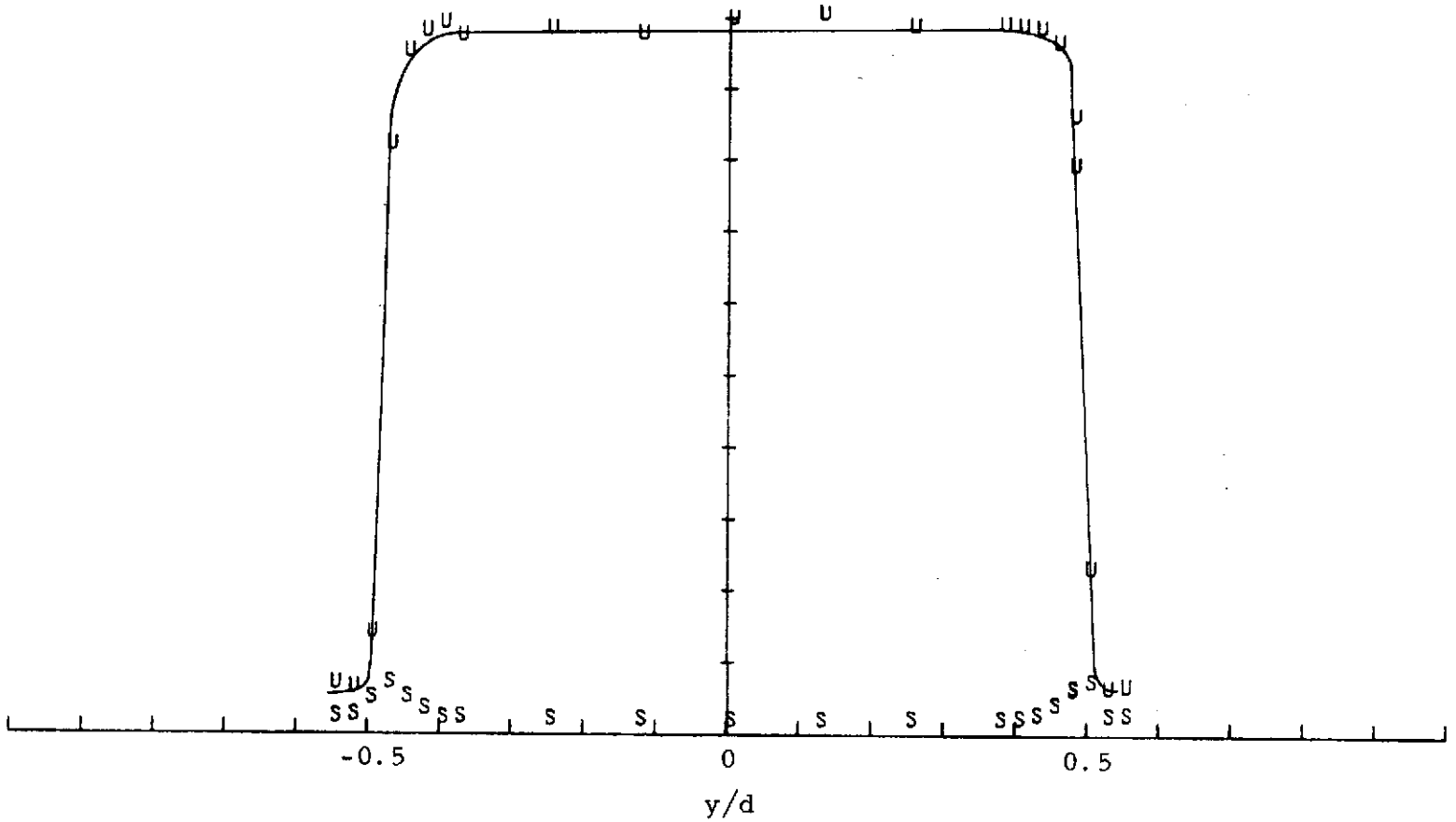

Figure 11. Mean velocity ratio, $U(0, y, 0)/U(0, 0, 0)$, and the relative intensity of the longitudinal fluctuation, $\tilde{u}(0, y, 0)$ for the conditions 0.4, 5, 930.

Note: Nominal mean velocity and r. m. s. relative intensity values are $U = 94.5 \pm 1$ fps and $\tilde{u} = 1.43 \pm 0.15$ percent. The tolerance values indicate the maximum deviations observed over the core region at the exit plane.

Comment: Misalignment of the jet tube array was apparently responsible for relative small core region. The resulting 3 inch tube boundary layer was responsible for the rounded mean velocity and increased $\tilde{u}$ values near edge of jet. This problem has been rectified.

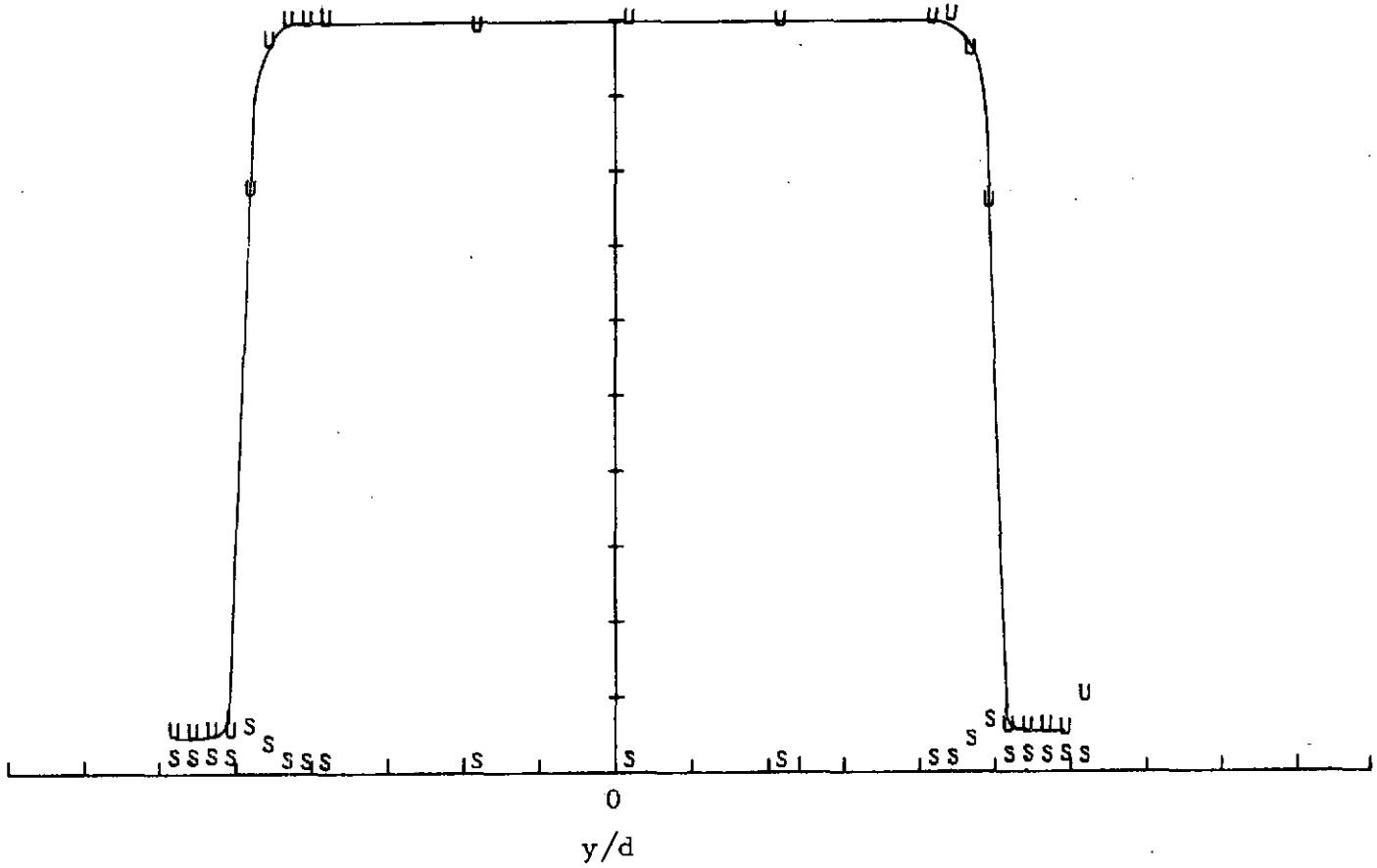

Figure 12. Mean velocity ratio, $U(0, y, 0)/U(0, 0, 0)$, and the relative intensity of the longitudinal fluctuation, $\tilde{u}(0, y, 0)$ for the conditions 0. 3, 5, 980.

Note: Nominal mean velocity and r. m. s. relative intensity values are $U = 103.8 \pm 0.5$ fps and $\tilde{u} = 0.8 \pm 0.1$ percent. The tolerance values indicate the maximum deviations observed over the core region at the exit plane.

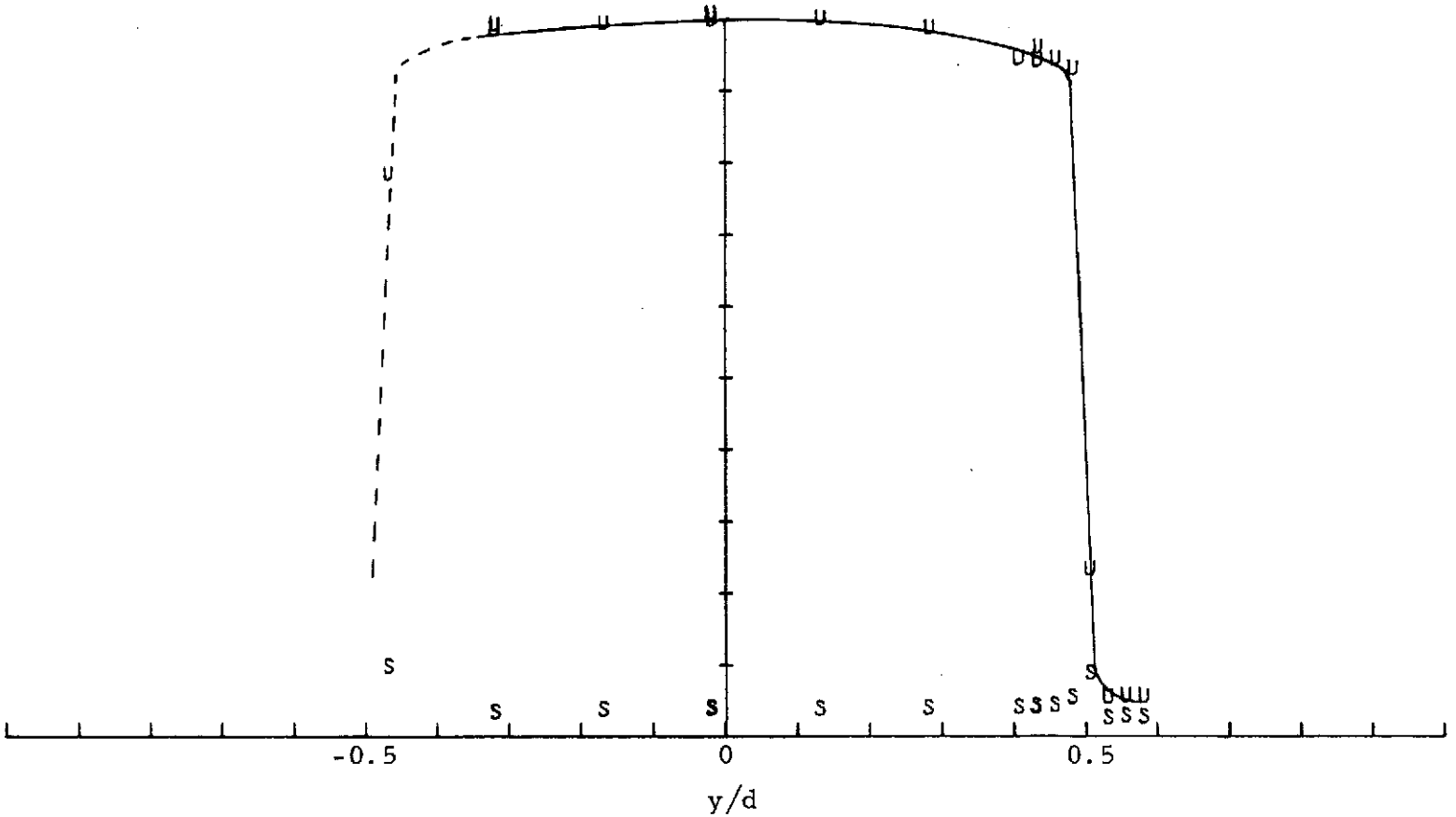

Figure 13. Mean velocity ratio, $U(0, y, 0)/U(0, 0, 0)$, and the relative intensity of the longitudinal fluctuation, $\tilde{u}(0, y, 0)$ for the conditions 0.5, 20, 0.

Note: Nominal mean velocity and r. m. s. relative intensity values are $U = 65.1 \pm 0.6$ fps and $\tilde{u} = 2.8 \pm 0.3$ percent. The tolerance values indicate the maximum deviations observed over the core region at the exit plane.

Comment: Nozzle exit flow results from jet-pump action of the tube array for the zero RPM condition. This apparently results in a minor rounding of the mean velocity profile. Note that $\tilde{u}$ distribution is not seriously effected for M = 0.5 but $\tilde{u}$ tolerance for M = 0.3 is approximately twice that of next largest.

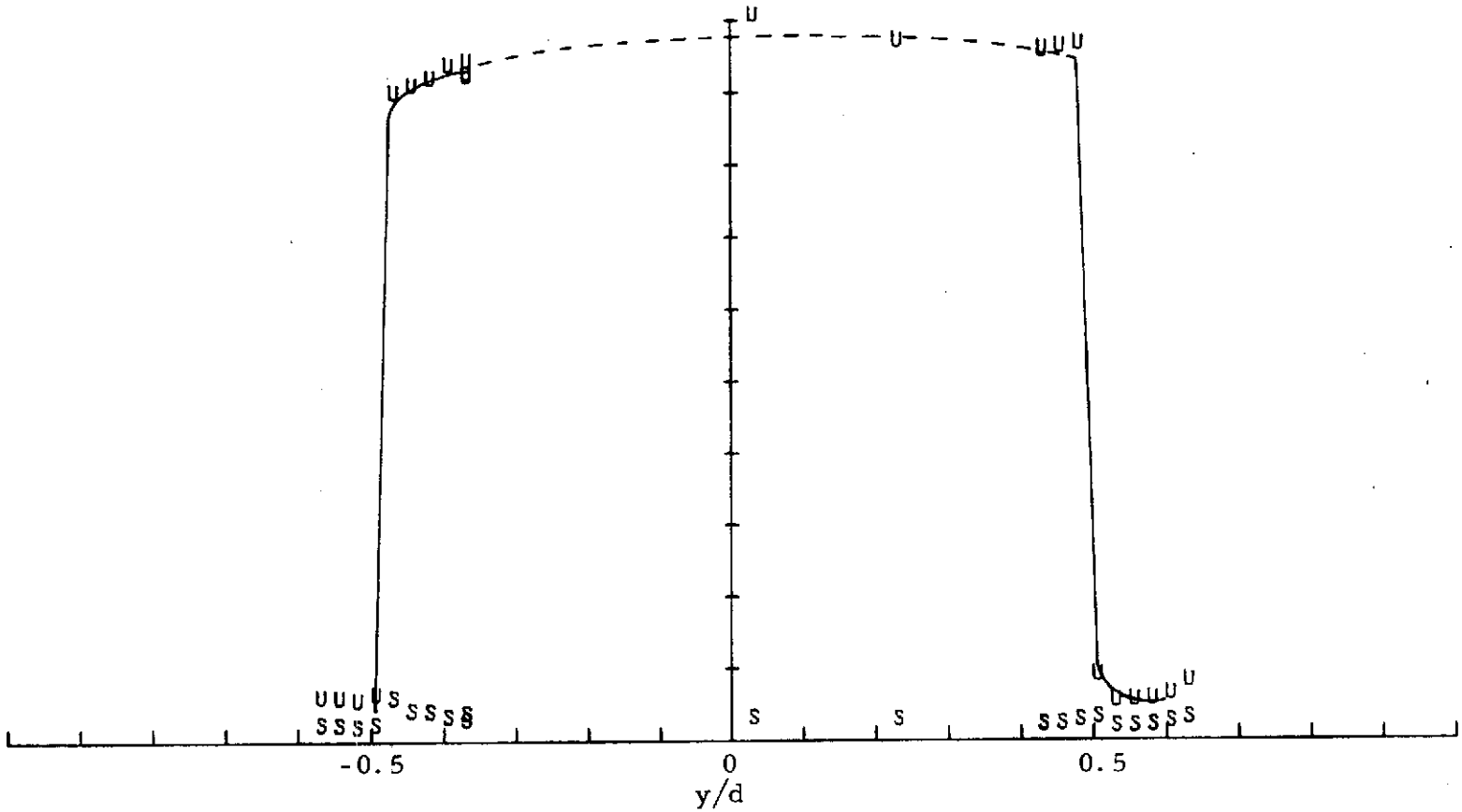

Figure 14. Mean velocity ratio, $U(0, y, 0)/U(0, 0, 0)$, and the relative intensity of the longitudinal fluctuation, $\tilde{u}(0, y, 0)$ for the conditions 0. 3, 15, 0.

Note: Nominal mean velocity and r. m. s. relative intensity values are $U = 60.5 \pm 1$ fps and $\tilde{u} = 1.85 \pm 0.35$ percent. The tolerance values indicate the maximum deviations observed over the core region at the exit plane.

Comment: Nozzle exit flow results from jet-pump action of the tube array for the zero RPM condition. This apparently results in a minor rounding of the mean velocity profile. Note that $\tilde{u}$ distribution is not seriously effected for M = 0. 5 but $\tilde{u}$ tolerance for M = 0. 3 is approximately twice that of next largest.

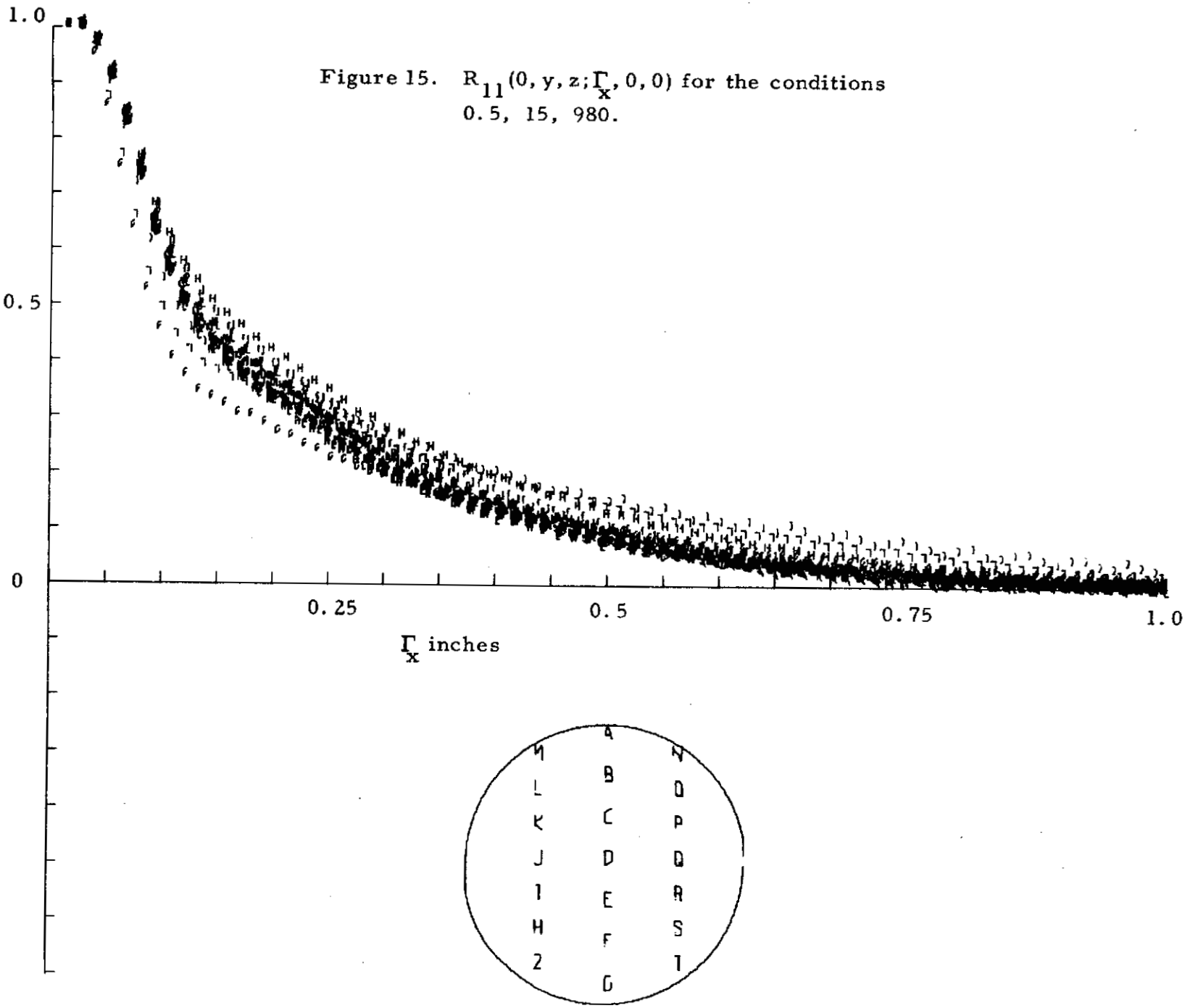

Figure 15. $R_{11}(0, y, z; \Gamma_x, 0, 0)$ for the conditions 0.5, 15, 980.

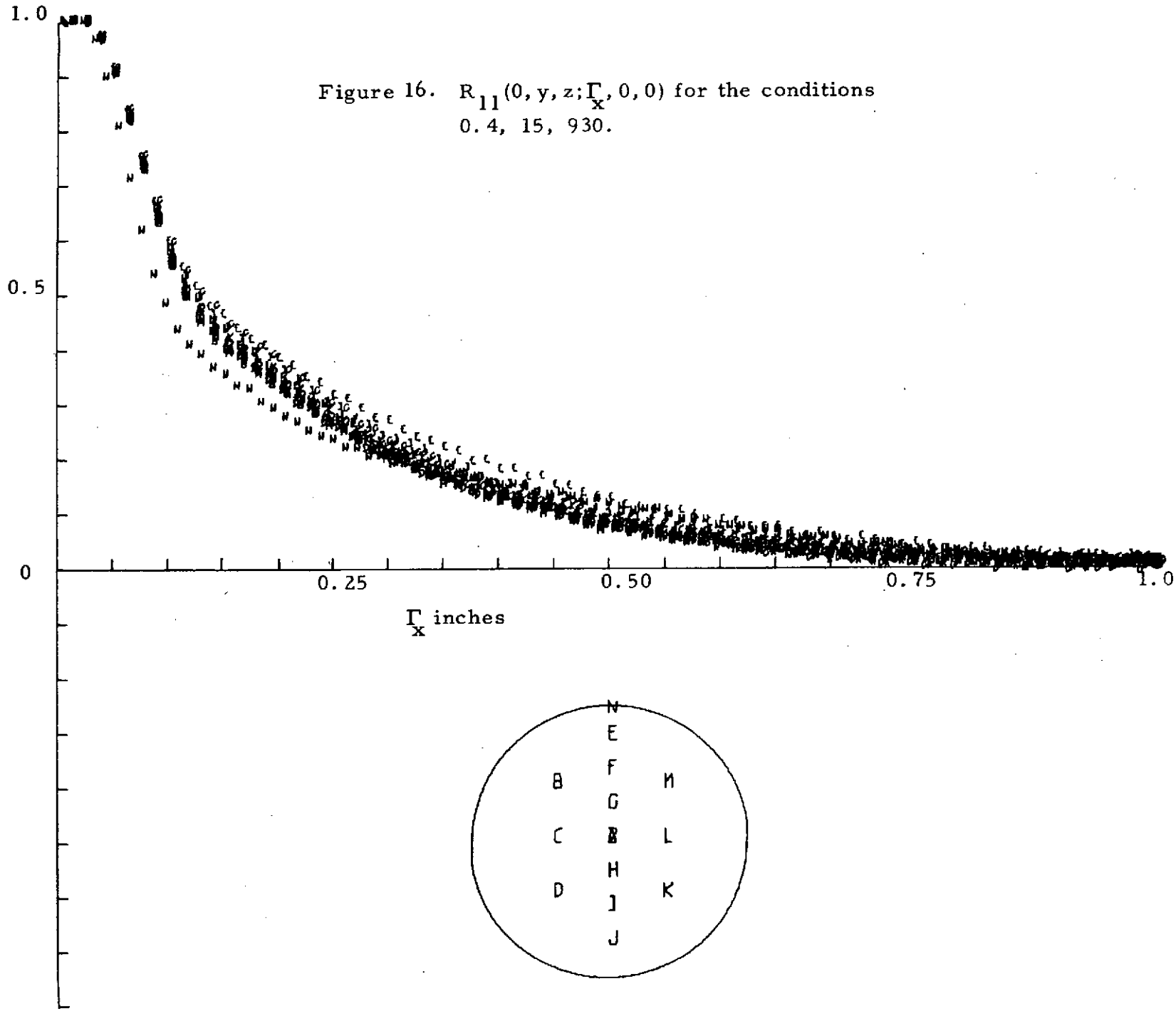

Figure 16. $R_{11}(0, y, z; \Gamma_x, 0, 0)$ for the conditions 0.4, 15, 930.

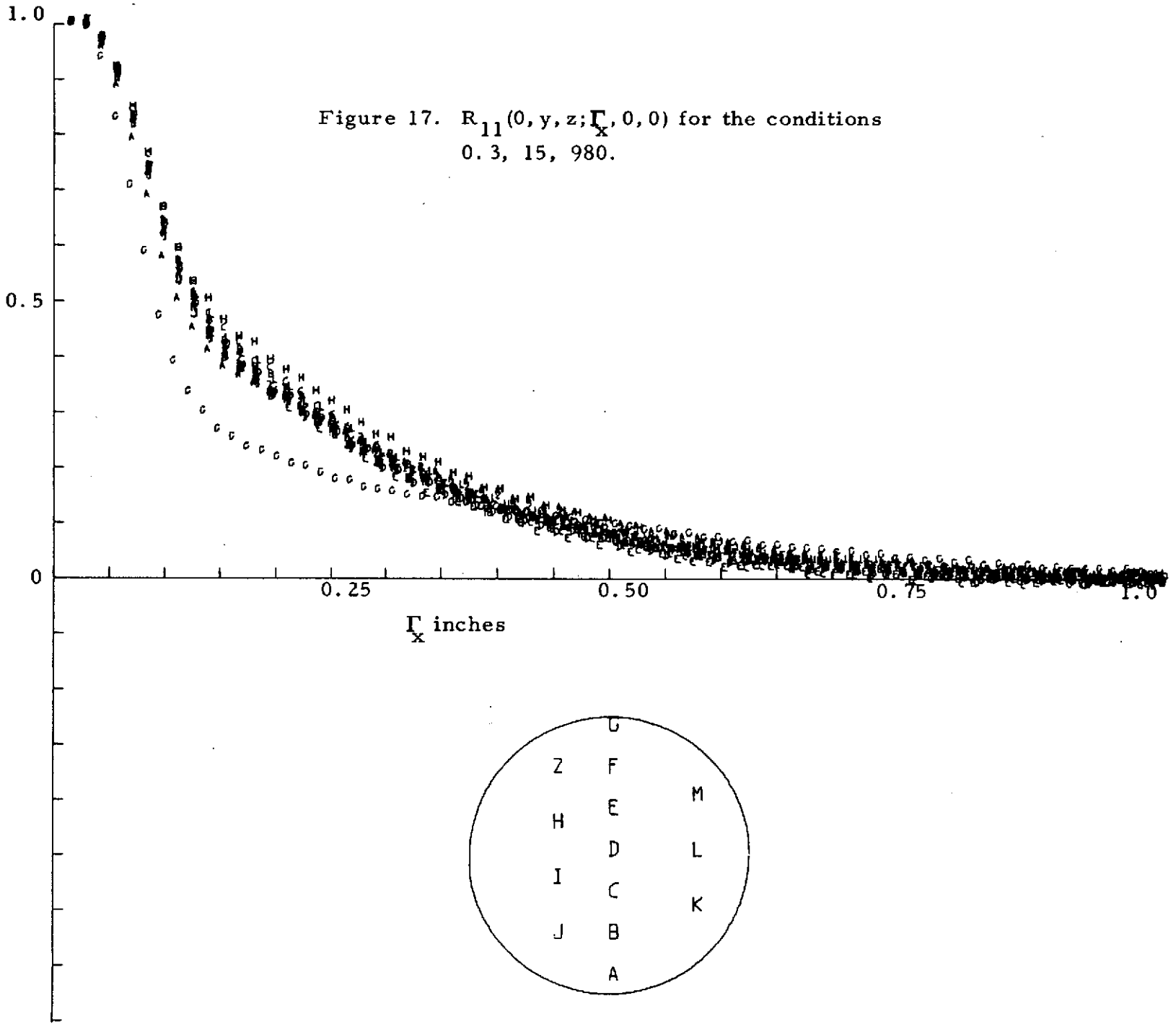

Figure 17. $R_{11}(0, y, z; \Gamma_x, 0, 0)$ for the conditions 0.3, 15, 980.

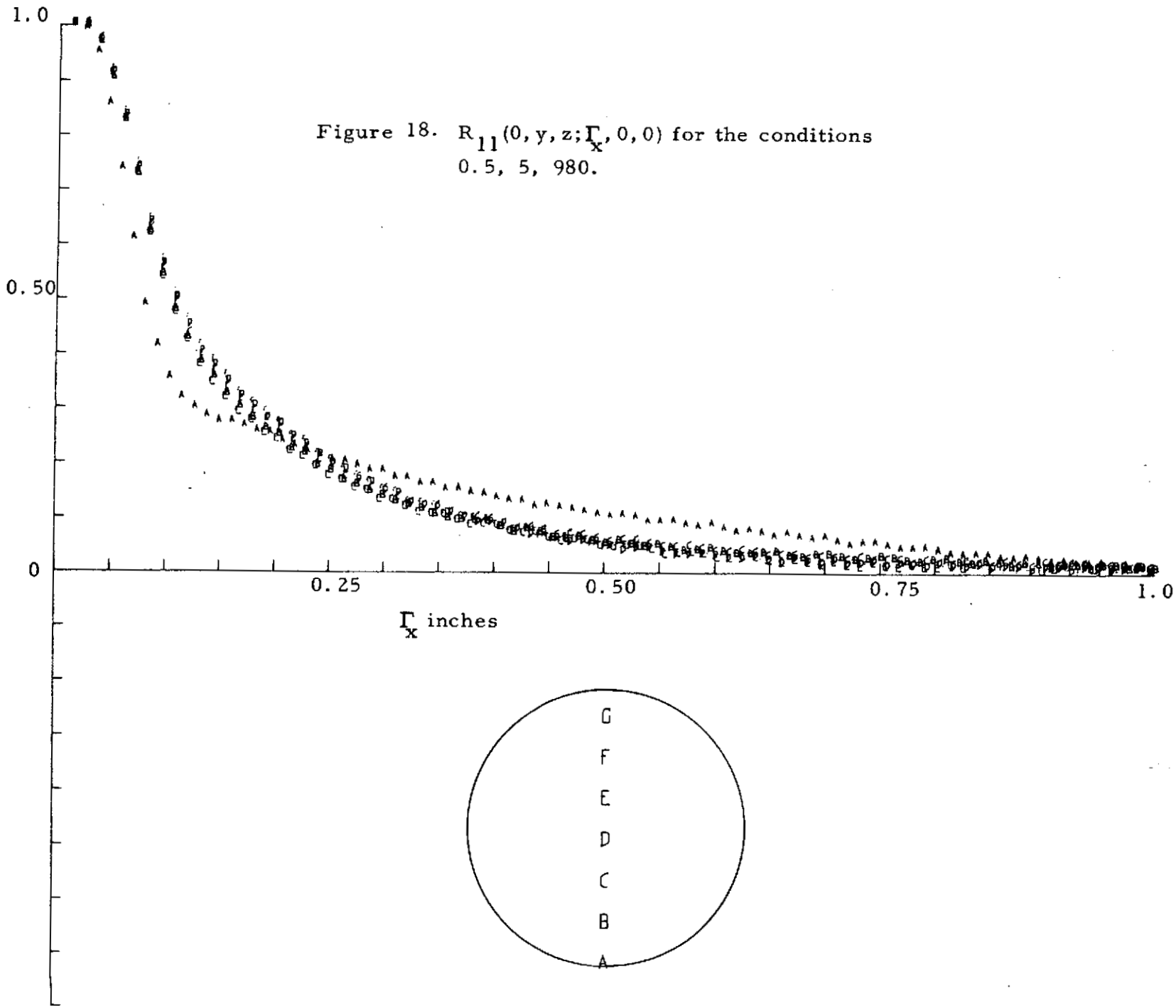

Figure 18. $R_{11}(0, y, z; \Gamma_x, 0, 0)$ for the conditions 0.5, 5, 980.

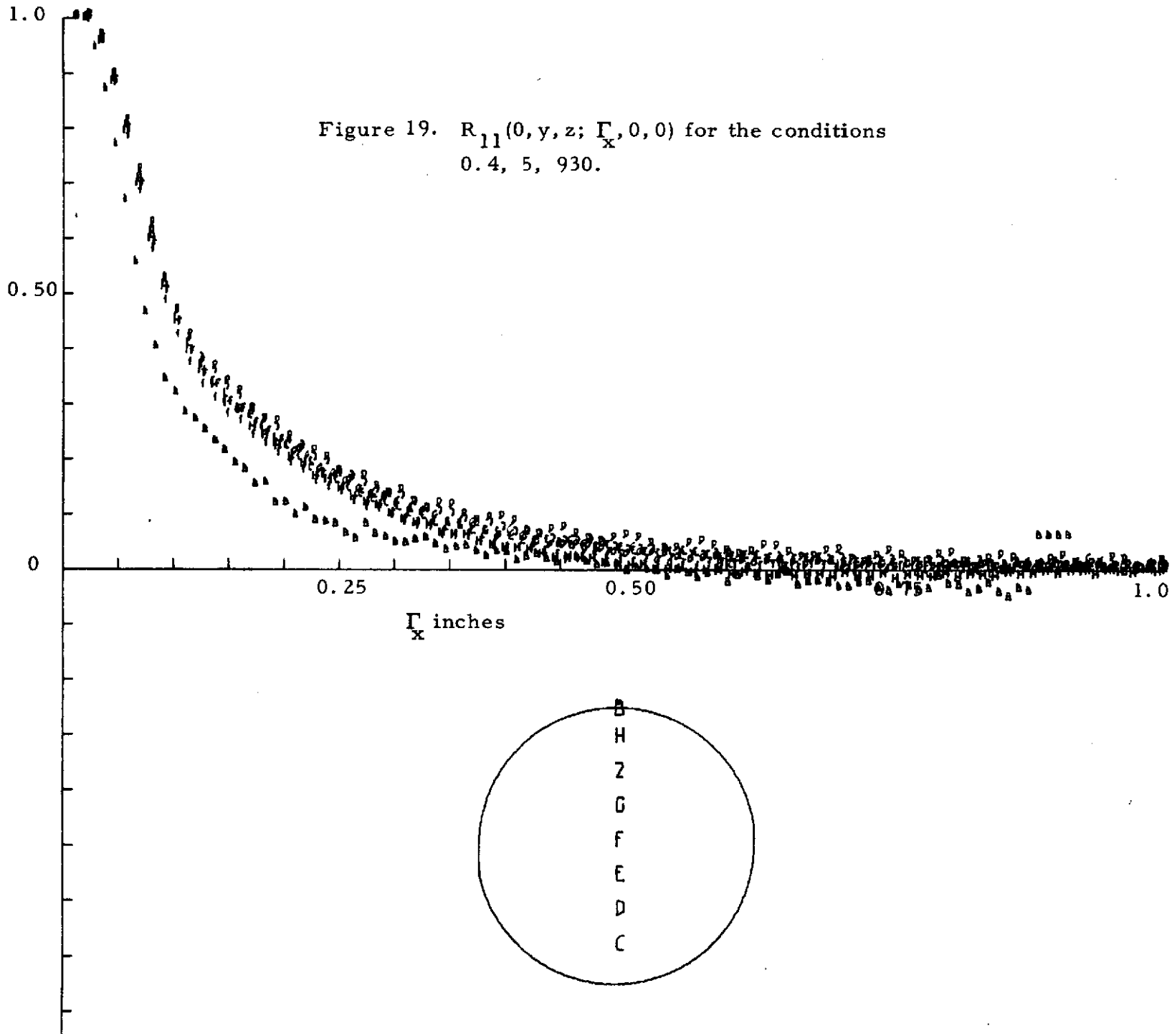

Figure 19. $R_{11}(0, y, z; \Gamma_x, 0, 0)$ for the conditions 0.4, 5, 930.

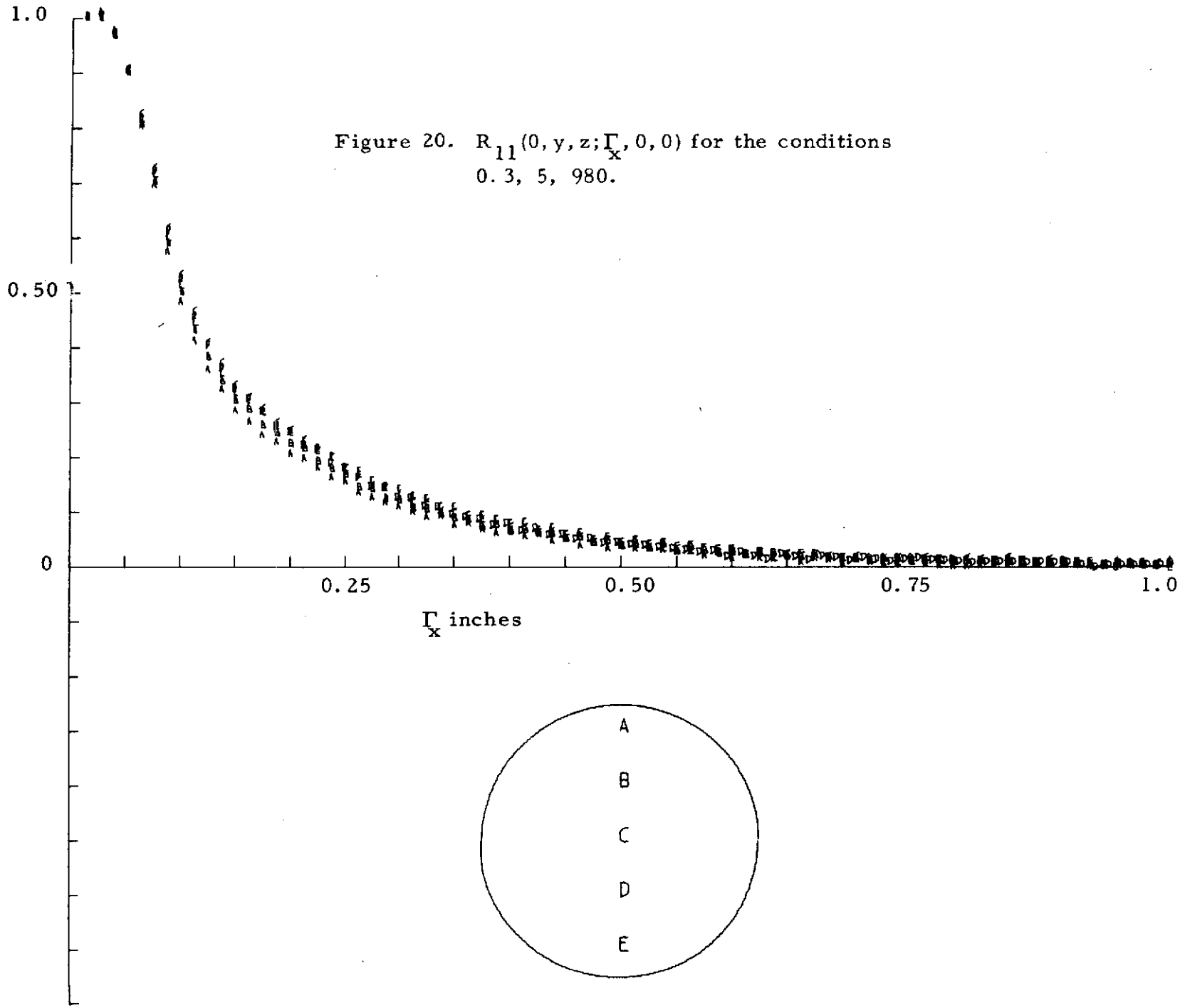

Figure 20. $R_{11}(0, y, z; \Gamma_x, 0, 0)$ for the conditions 0.3, 5, 980.

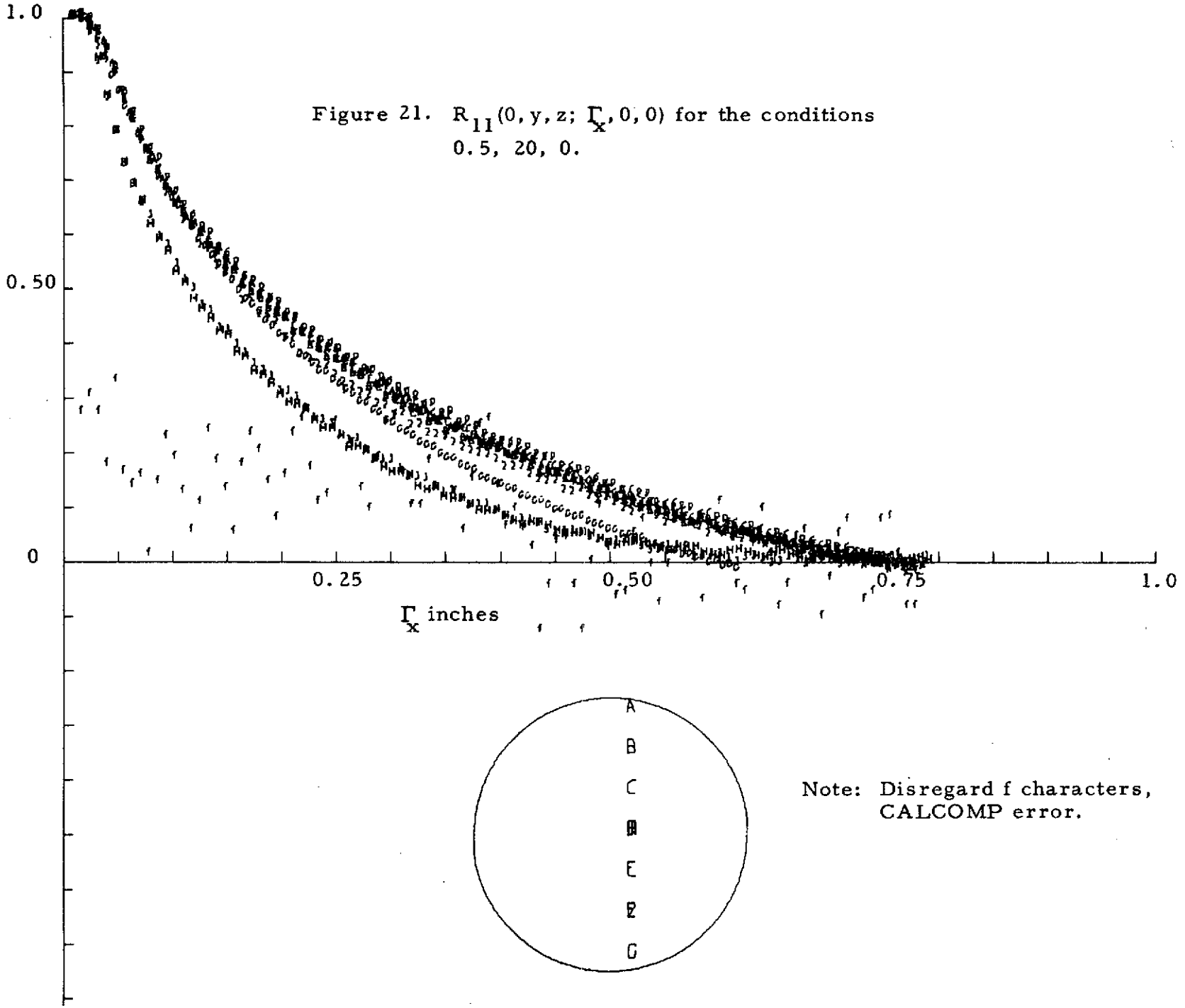

Figure 21. $R_{11}(0, y, z; \Gamma_x, 0, 0)$ for the conditions 0.5, 20, 0.

Note: Disregard f characters, CALCOMP error.

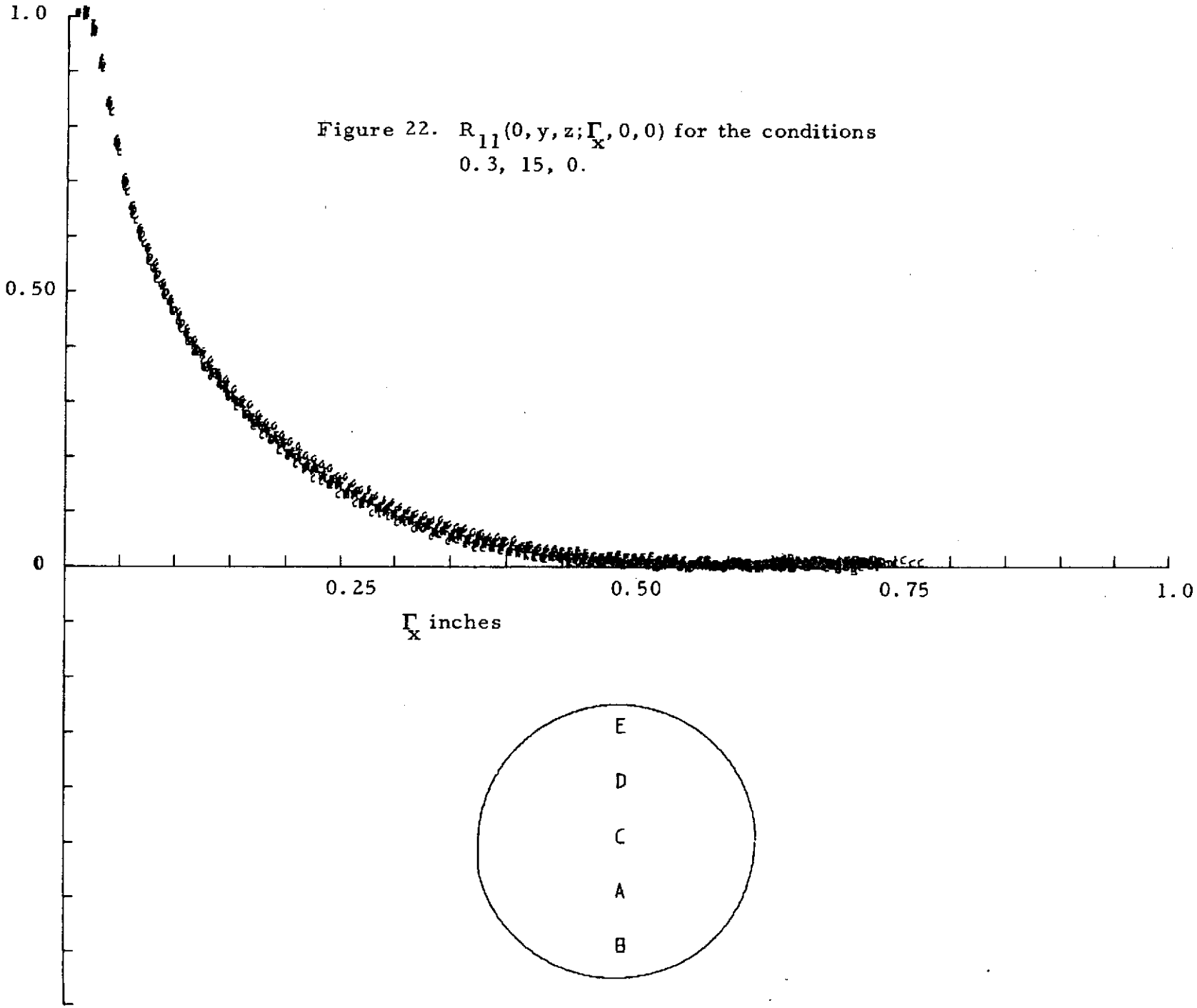

Figure 22. $R_{11}(0, y, z; \Gamma_x, 0, 0)$ for the conditions 0.3, 15, 0.

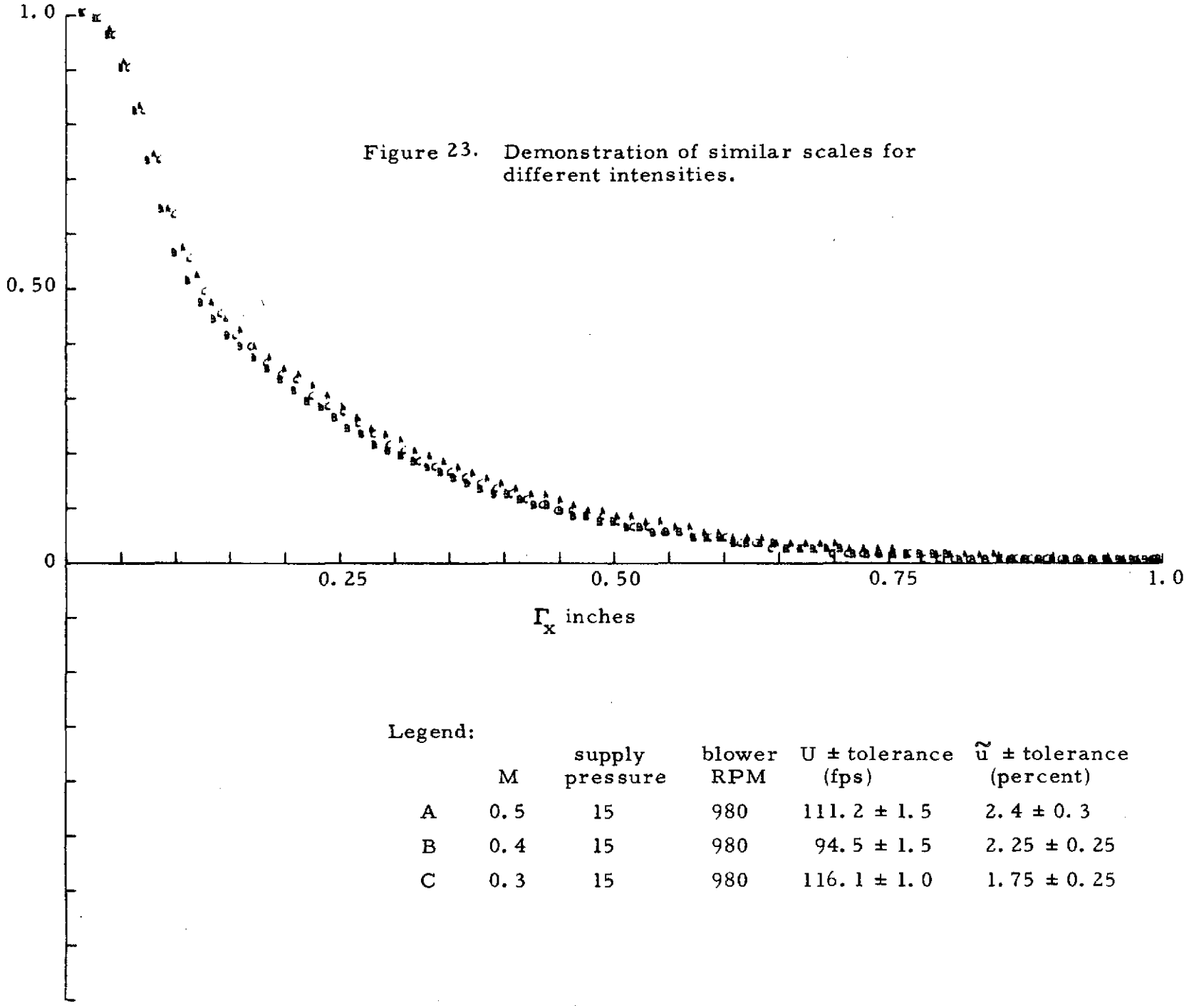

Figure 23. Demonstration of similar scales for different intensities.

Legend:

	M	supply pressure	blower RPM	U ± tolerance (fps)	$\tilde{u}$ ± tolerance (percent)
A	0.5	15	980	111.2 ± 1.5	2.4 ± 0.3
B	0.4	15	980	94.5 ± 1.5	2.25 ± 0.25
C	0.3	15	980	116.1 ± 1.0	1.75 ± 0.25

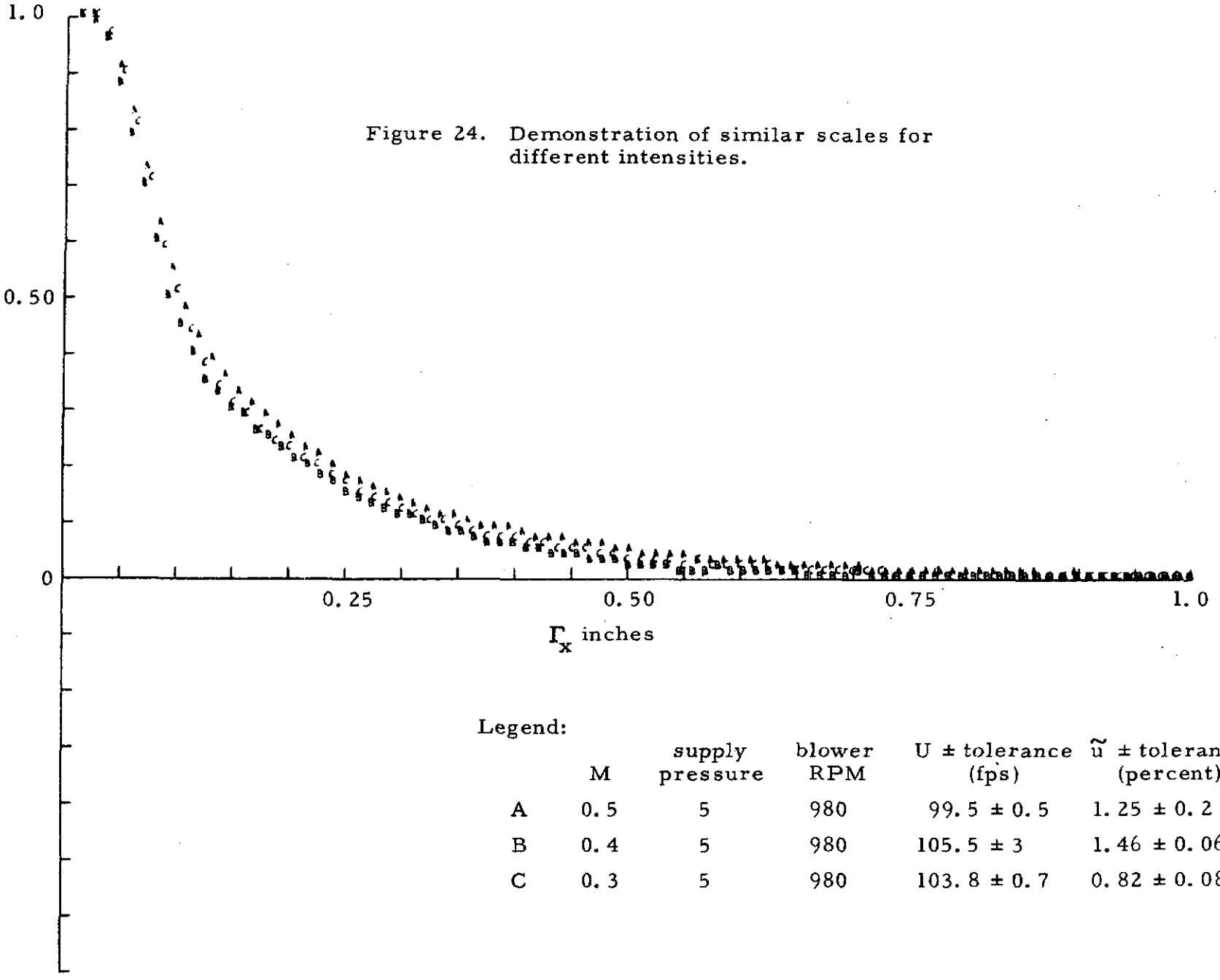

Figure 24. Demonstration of similar scales for different intensities.

Legend:

	M	supply pressure	blower RPM	U ± tolerance (fps)	$\tilde{u}$ ± tolerance (percent)
A	0.5	5	980	99.5 ± 0.5	1.25 ± 0.2
B	0.4	5	980	105.5 ± 3	1.46 ± 0.06
C	0.3	5	980	103.8 ± 0.7	0.82 ± 0.08

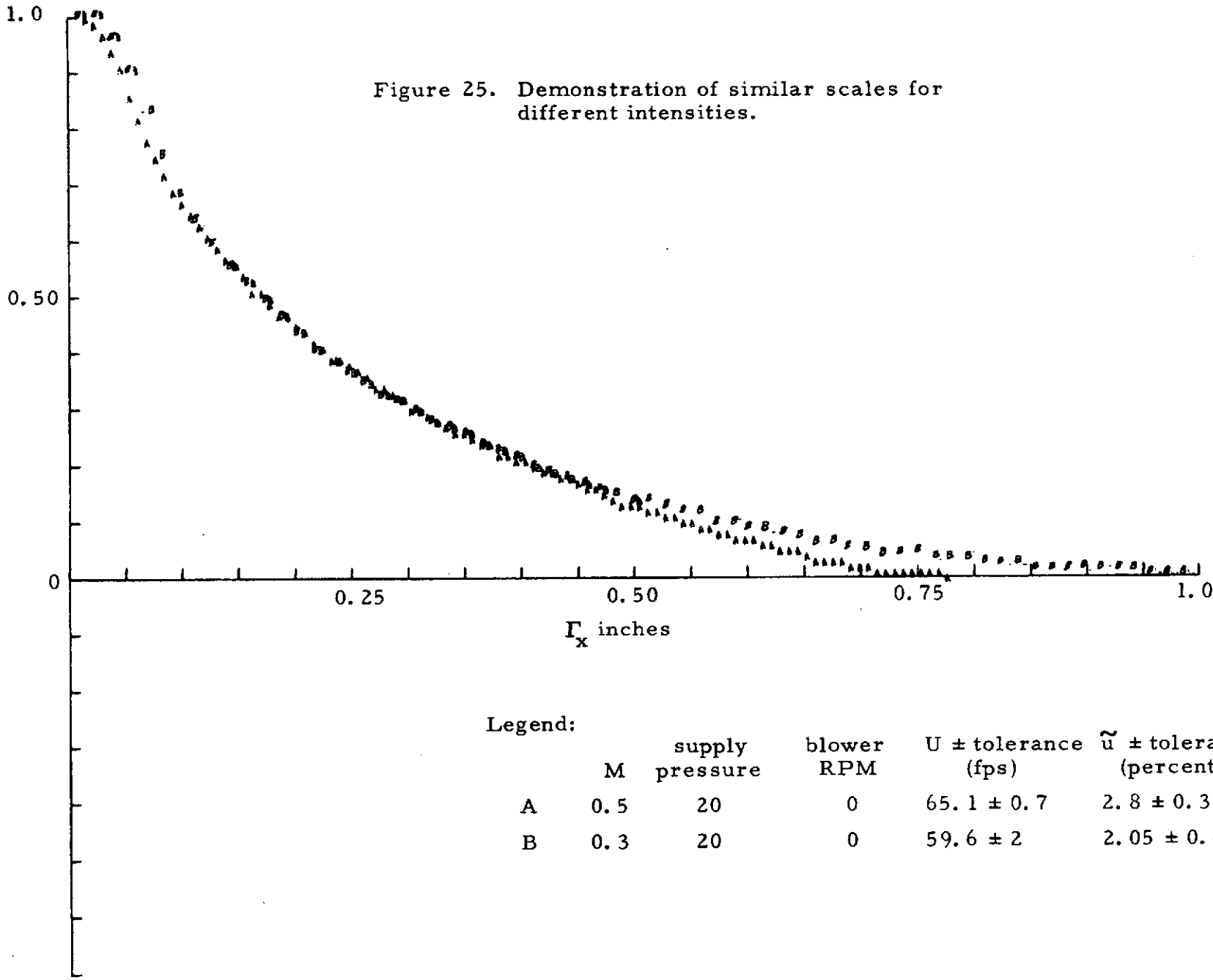

Figure 25. Demonstration of similar scales for different intensities.

Legend:

	M	supply pressure	blower RPM	U ± tolerance (fps)	$\tilde{u}$ ± tolerance (percent)
A	0.5	20	0	65.1 ± 0.7	2.8 ± 0.3
B	0.3	20	0	59.6 ± 2	2.05 ± 0.45

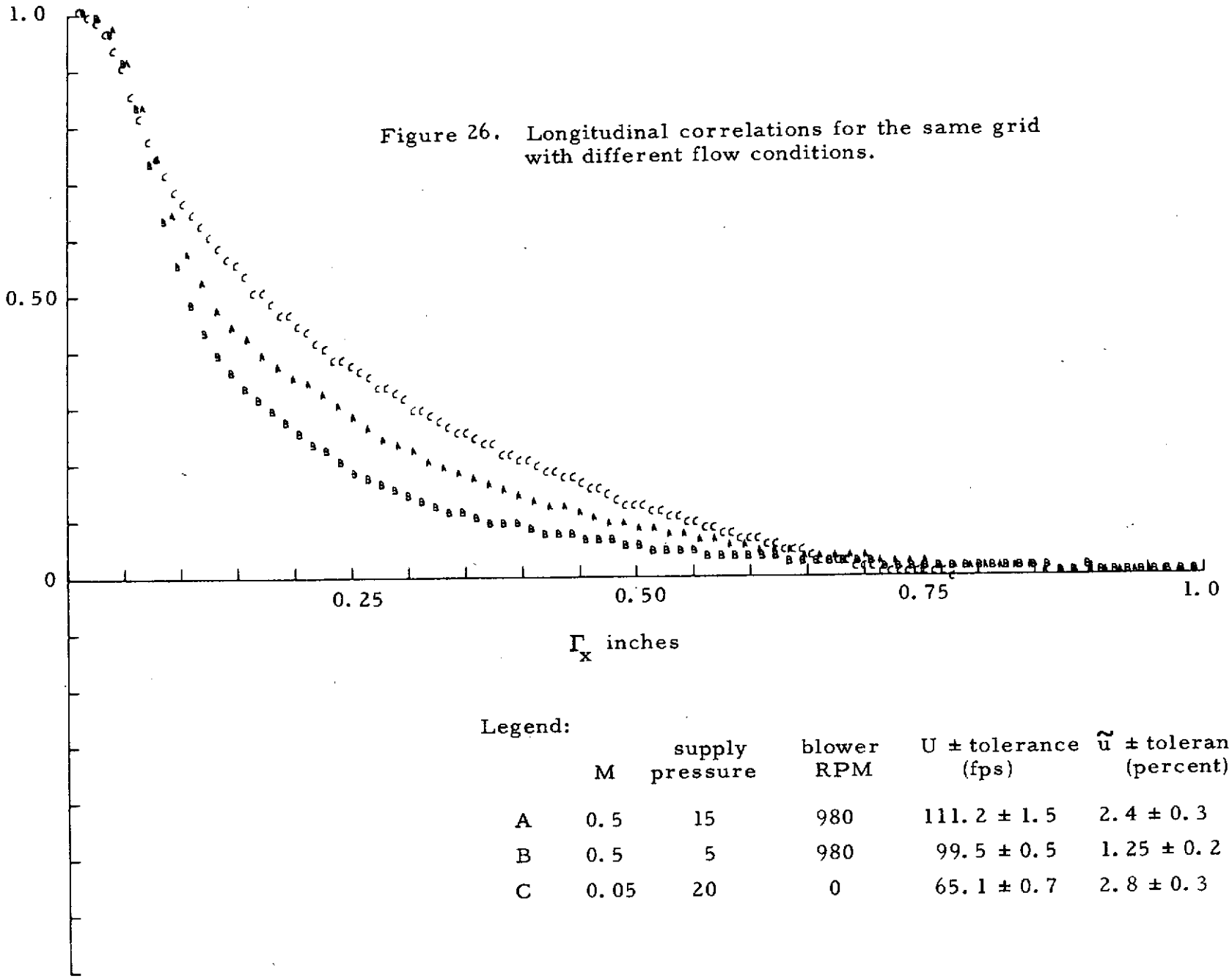

Figure 26. Longitudinal correlations for the same grid with different flow conditions.

Legend:

	M	supply pressure	blower RPM	U ± tolerance (fps)	$\tilde{u}$ ± tolerance (percent)
A	0.5	15	980	111.2 ± 1.5	2.4 ± 0.3
B	0.5	5	980	99.5 ± 0.5	1.25 ± 0.2
C	0.05	20	0	65.1 ± 0.7	2.8 ± 0.3

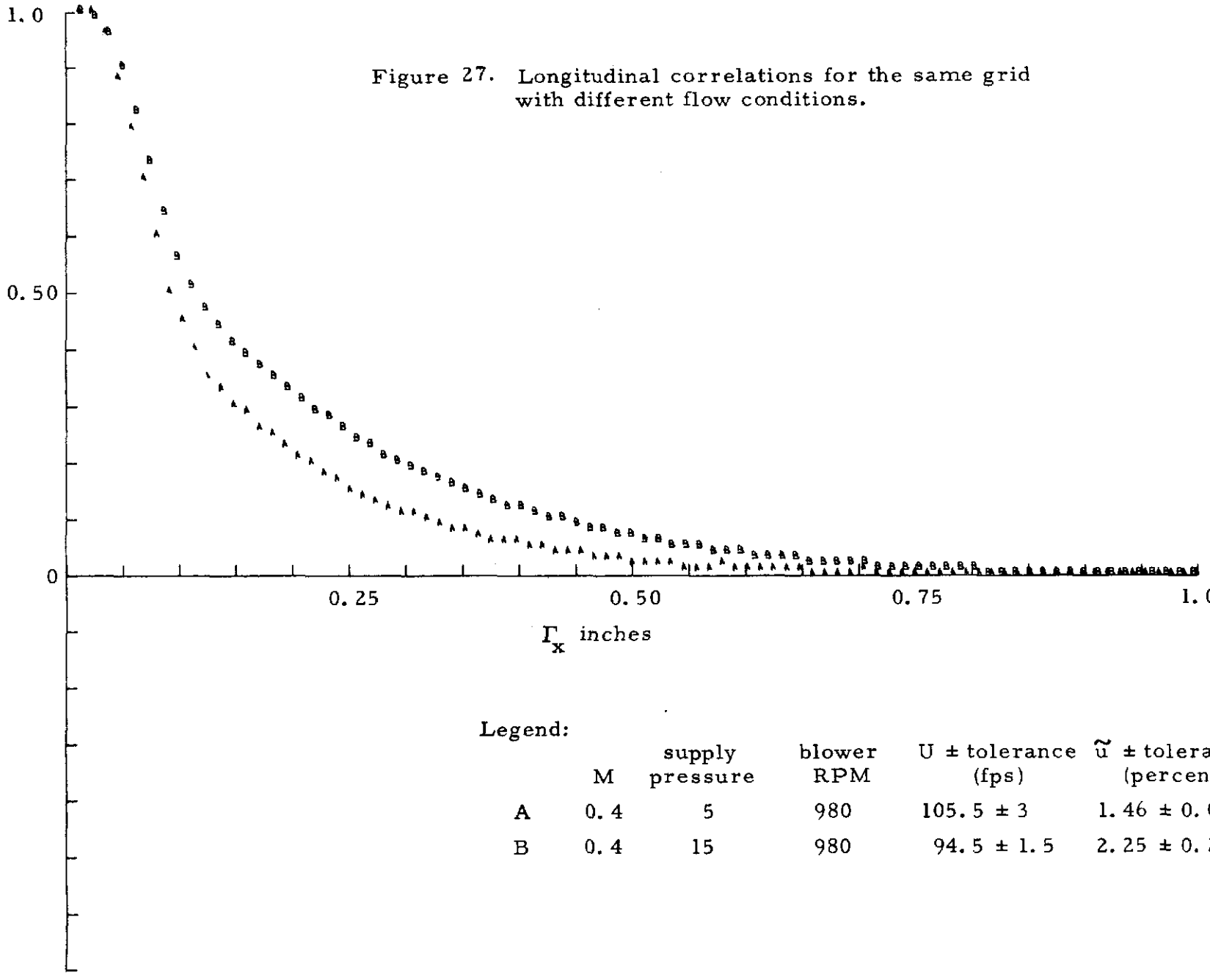

Figure 27. Longitudinal correlations for the same grid with different flow conditions.

Legend:

	M	supply pressure	blower RPM	U ± tolerance (fps)	$\tilde{u}$ ± tolerance (percent)
A	0.4	5	980	105.5 ± 3	1.46 ± 0.06
B	0.4	15	980	94.5 ± 1.5	2.25 ± 0.25

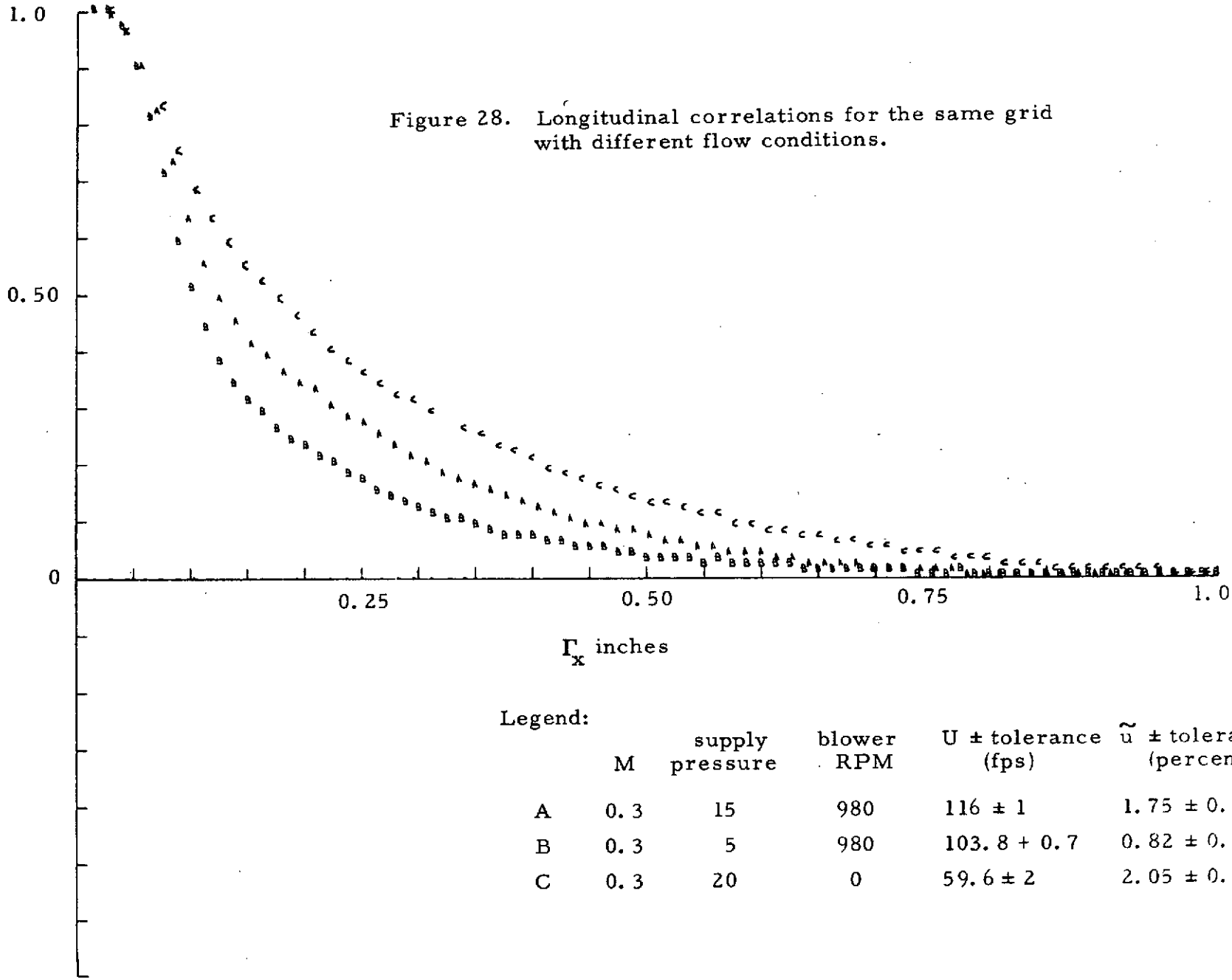

Figure 28. Longitudinal correlations for the same grid with different flow conditions.

Legend:

	M	supply pressure	blower RPM	U ± tolerance (fps)	$\tilde{u}$ ± tolerance (percent)
A	0.3	15	980	116 ± 1	1.75 ± 0.25
B	0.3	5	980	103.8 + 0.7	0.82 ± 0.08
C	0.3	20	0	59.6 ± 2	2.05 ± 0.45

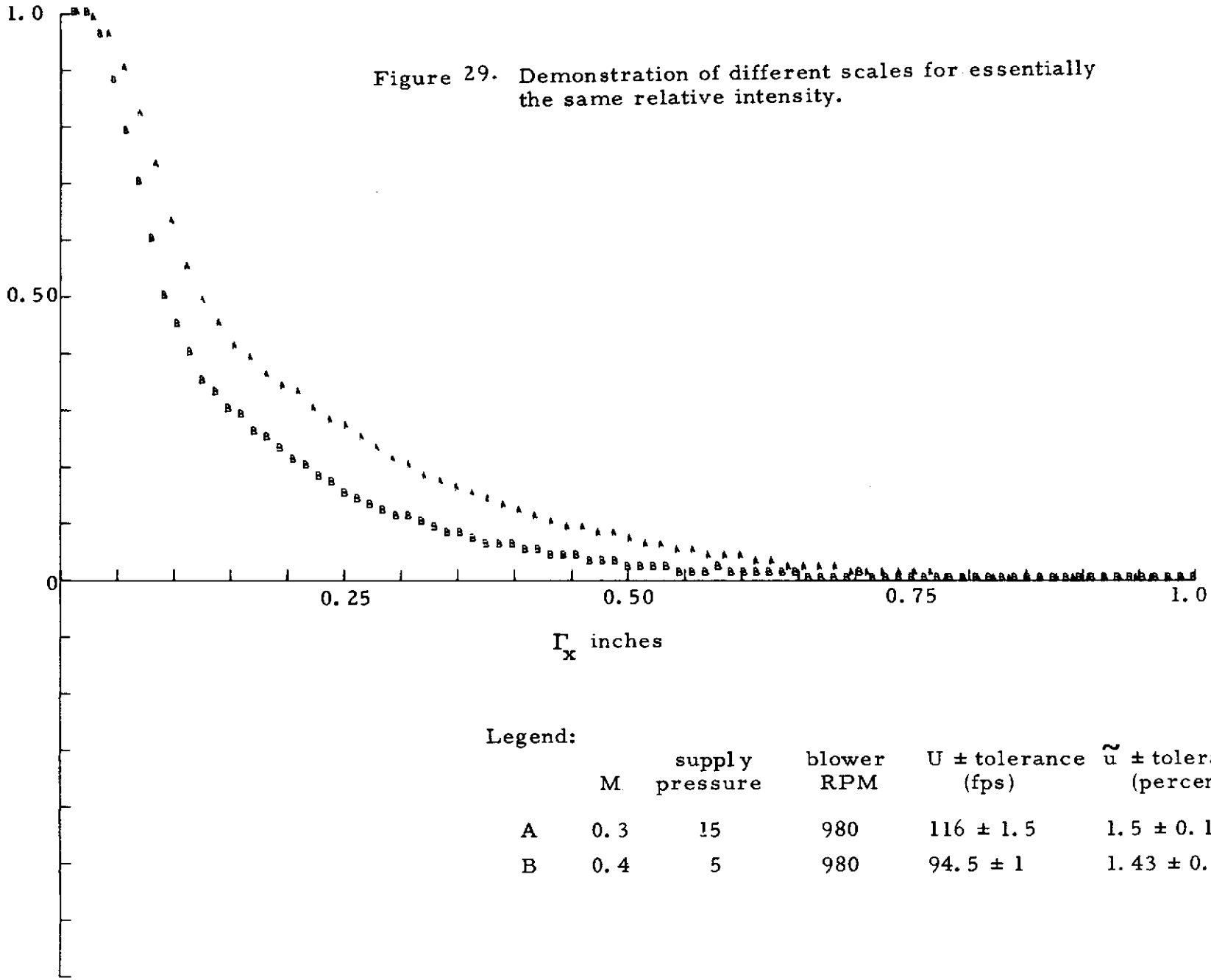

Figure 29. Demonstration of different scales for essentially the same relative intensity.

Legend:

	M	supply pressure	blower RPM	U ± tolerance (fps)	$\tilde{u}$ ± tolerance (percent)
A	0.3	15	980	116 ± 1.5	1.5 ± 0.1
B	0.4	5	980	94.5 ± 1	1.43 ± 0.15

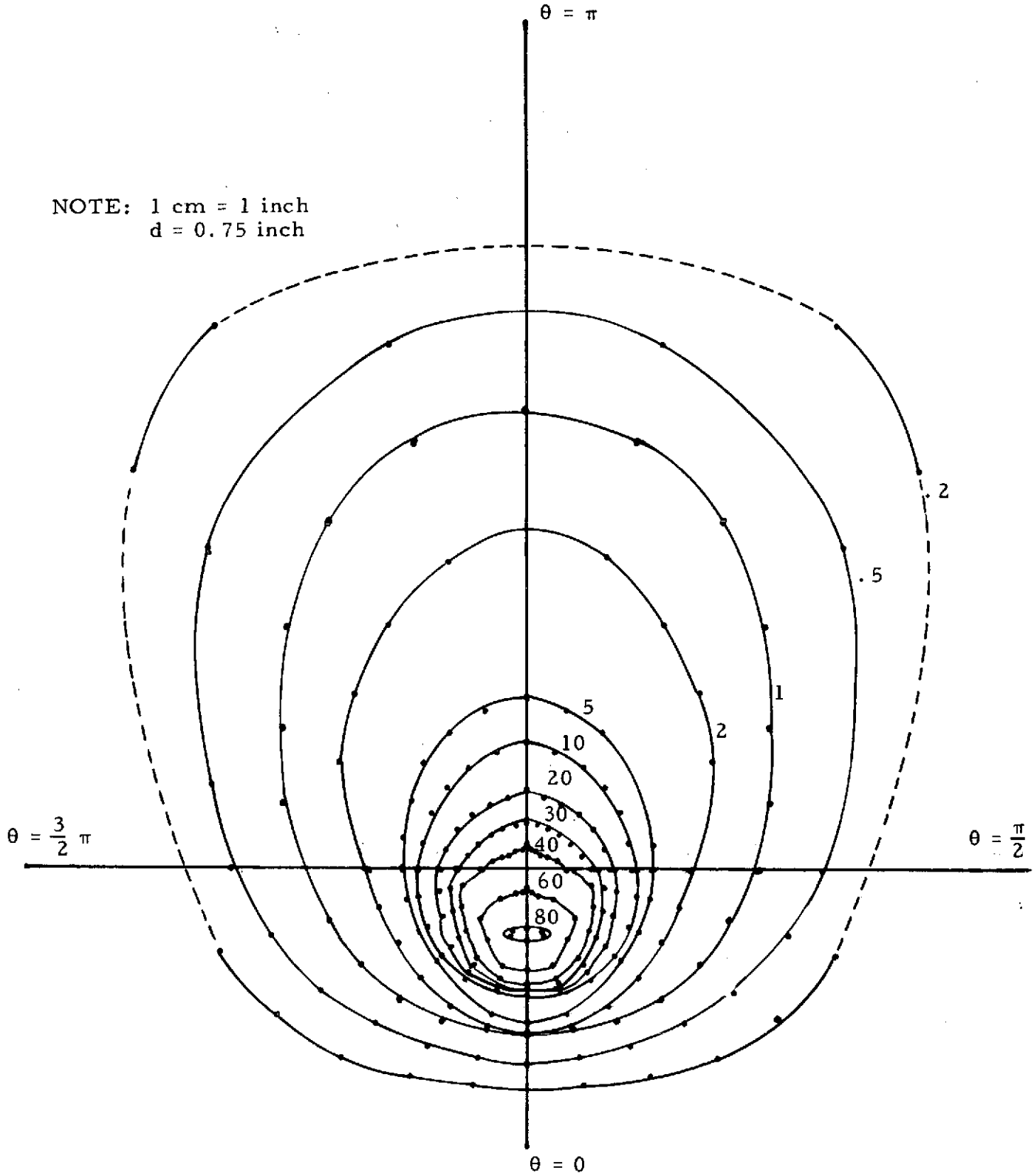

a) Complete data set.

Figure 30. Surface pressure isobar contours for the case $\alpha = 45^{\circ}$, $L/d = 2.12$, jet Reynolds number $= 4.8 \times 10^4$.

Contours represent level curves of $100 \dfrac{(p - p_{atm})}{u_p^2 \lambda \sin\alpha}$

$\lambda = \int_{A_{jet}} \rho u^2 dA / \rho u_p^2 A_{jet}$, $\lambda = 0.809$ taken from [1]

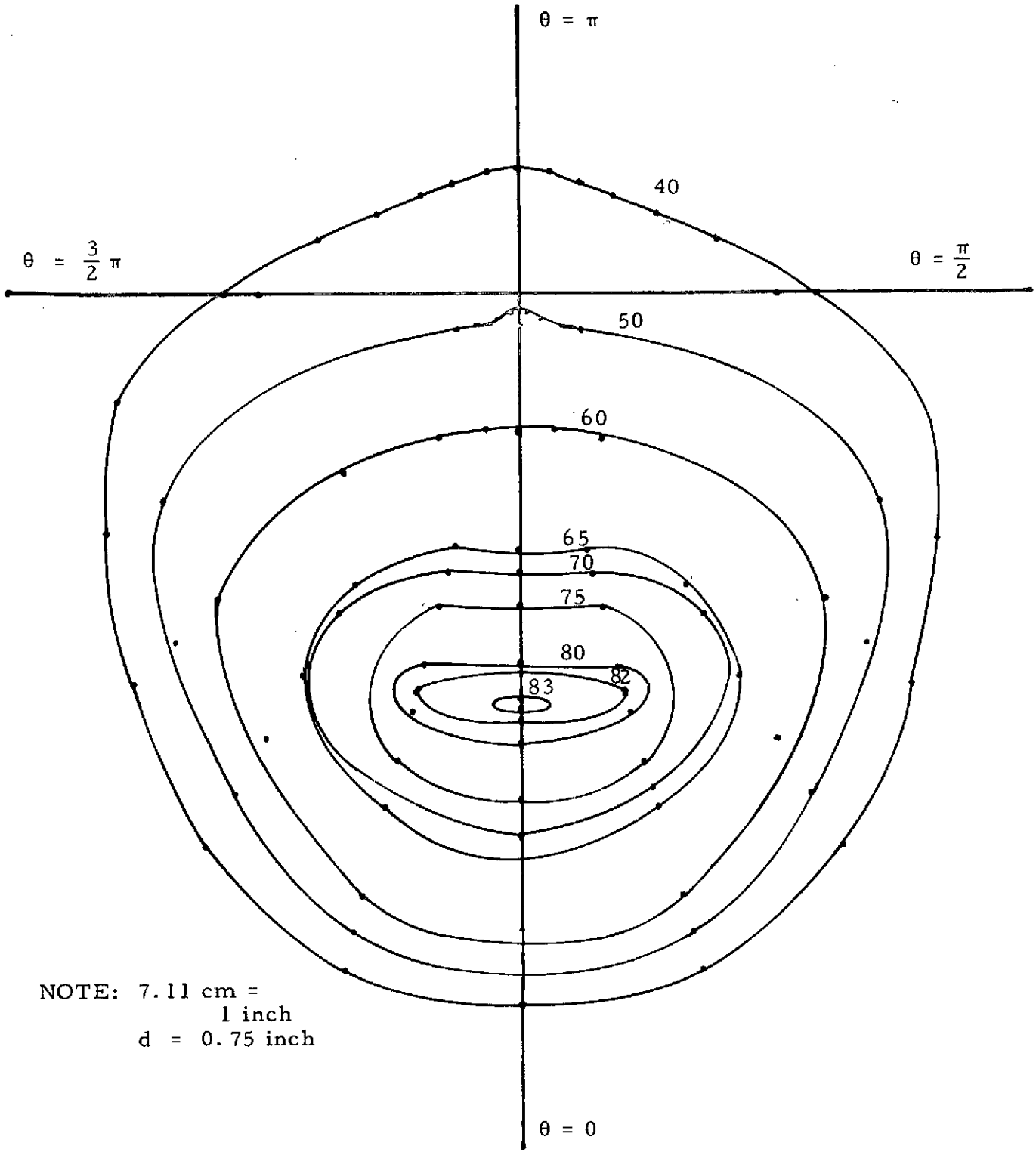

b) Expanded scale to show detail of maximum pressure region.

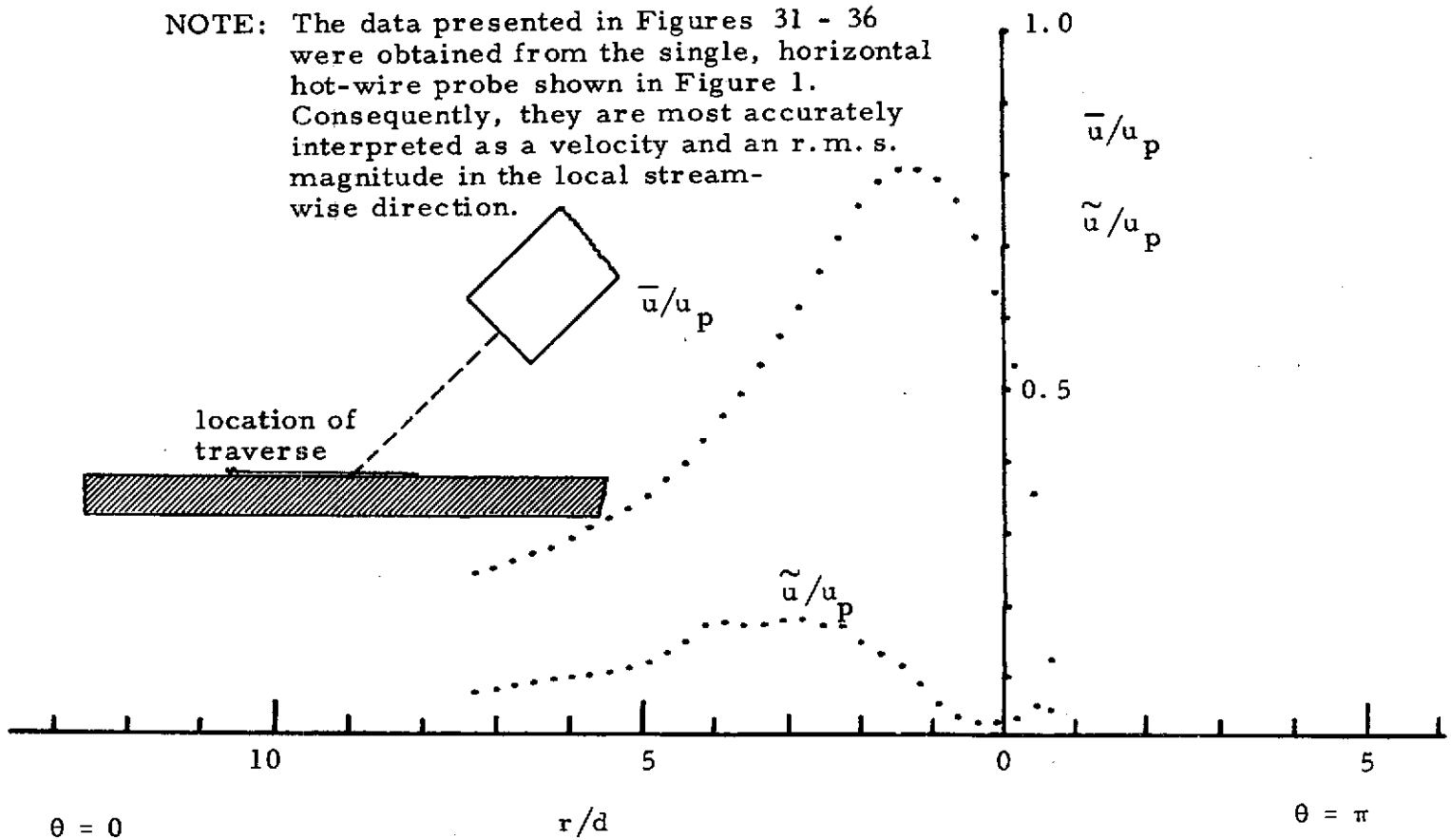

Figure 31. $\overline{u}/u_p$, $\tilde{u}/u_p$ vs r for the $\theta = 0$ plane, $z/d = 0.0133$.
($L/d = 2.12$, $d = 0.75$ inches)

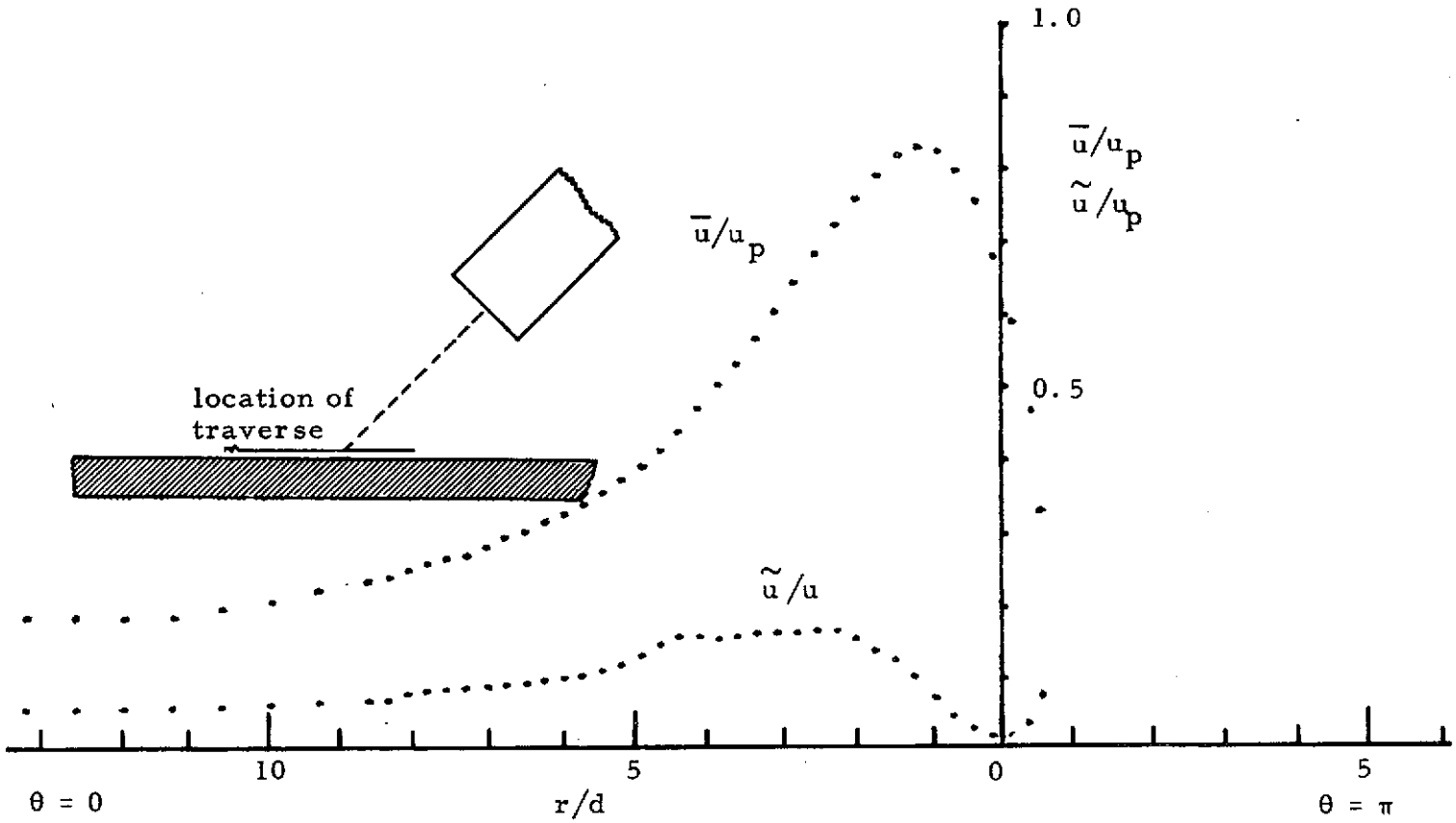

Figure 32. $\bar{u}/u_p$, $\tilde{u}/u_p$ vs r for the θ = 0 plane, z/d = 0.0833.
(L/d = 2.12, d = 0.75 inches)

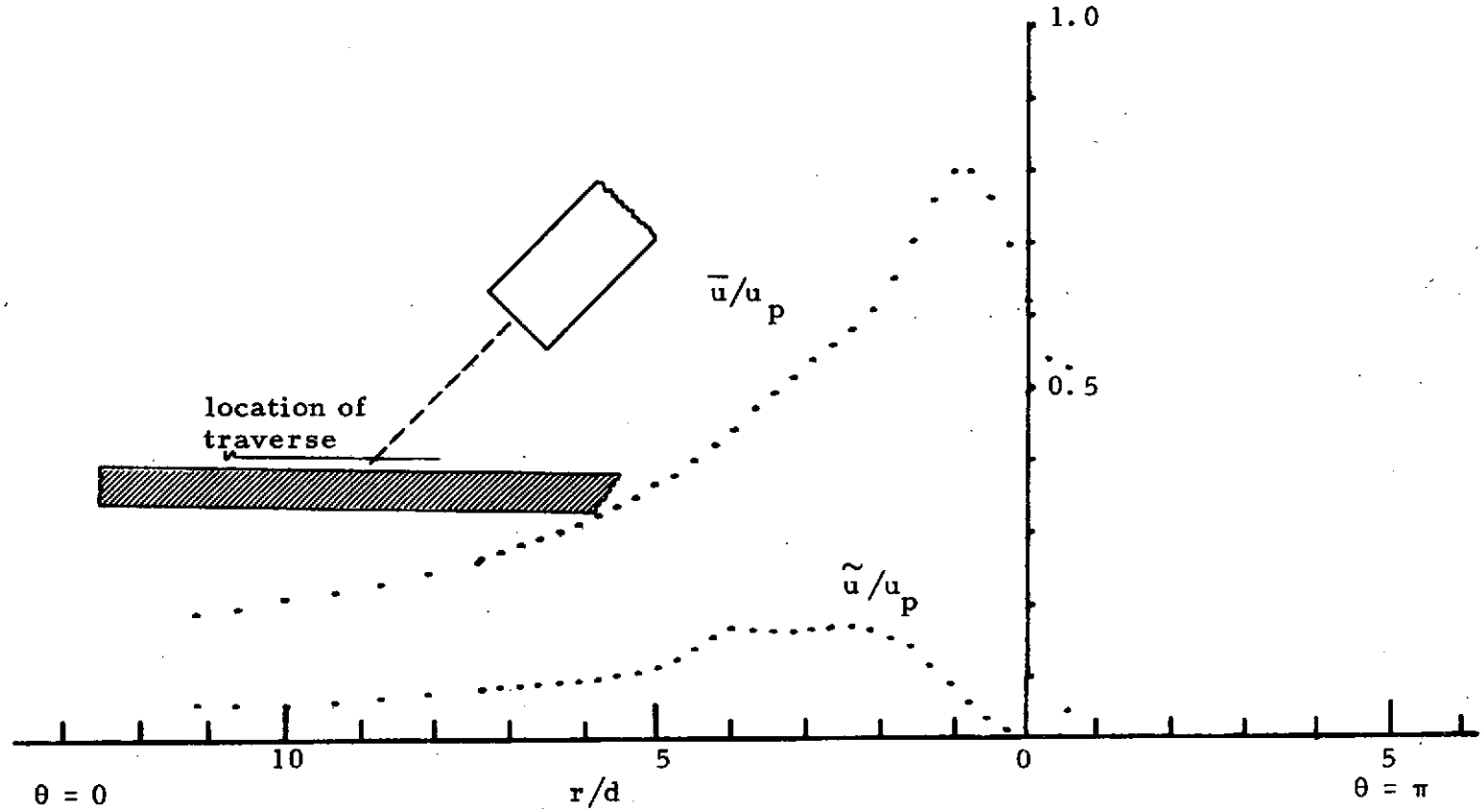

Figure 33. $\bar{u}/u_p$, $\tilde{u}/u_p$ vs r for the θ = 0 plane, z/d = 0.166.
(L/d = 2.12, d = 0.75 inches)

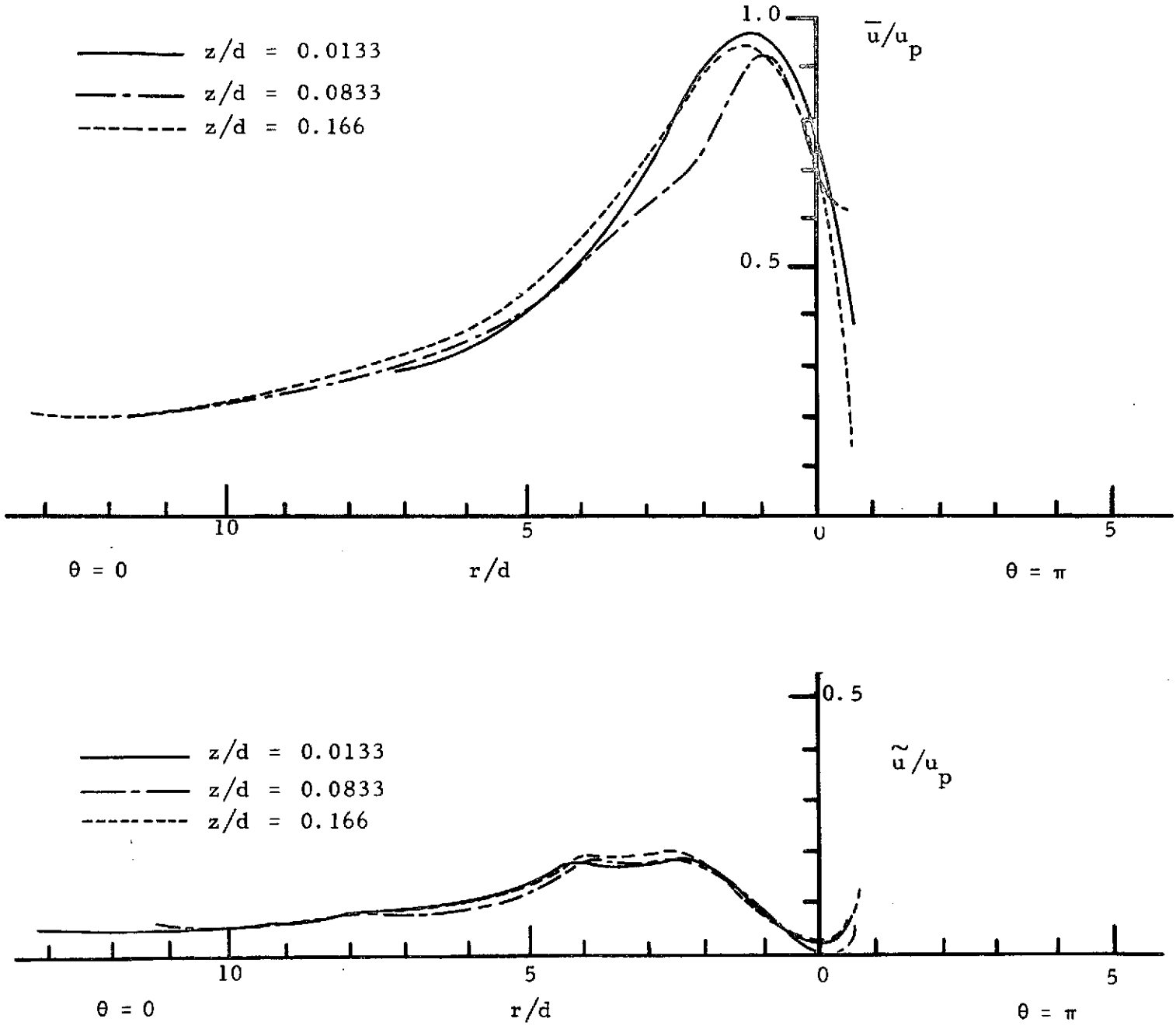

Figure 34. Comparison of radial traverse data from three z/d locations.

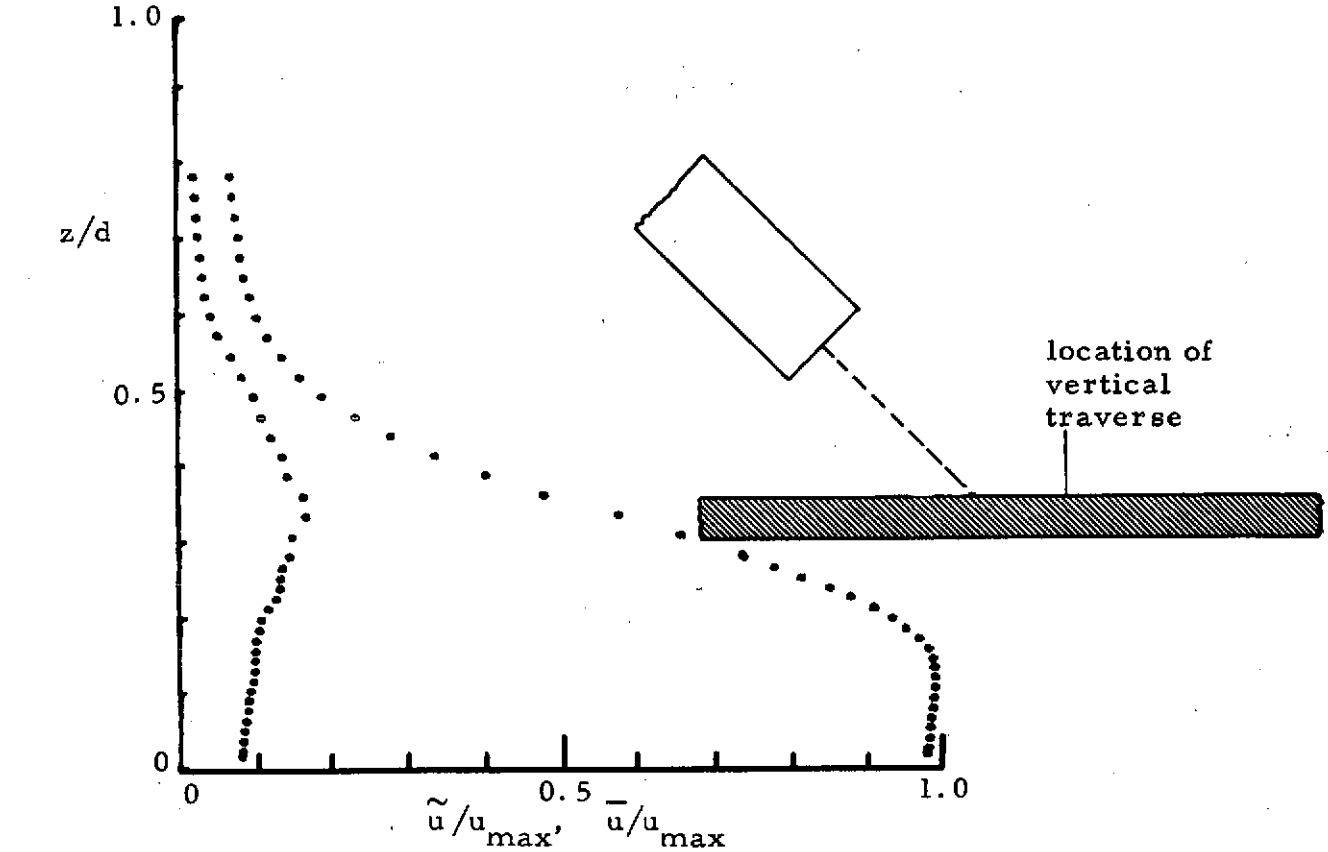

a) r/d = 1

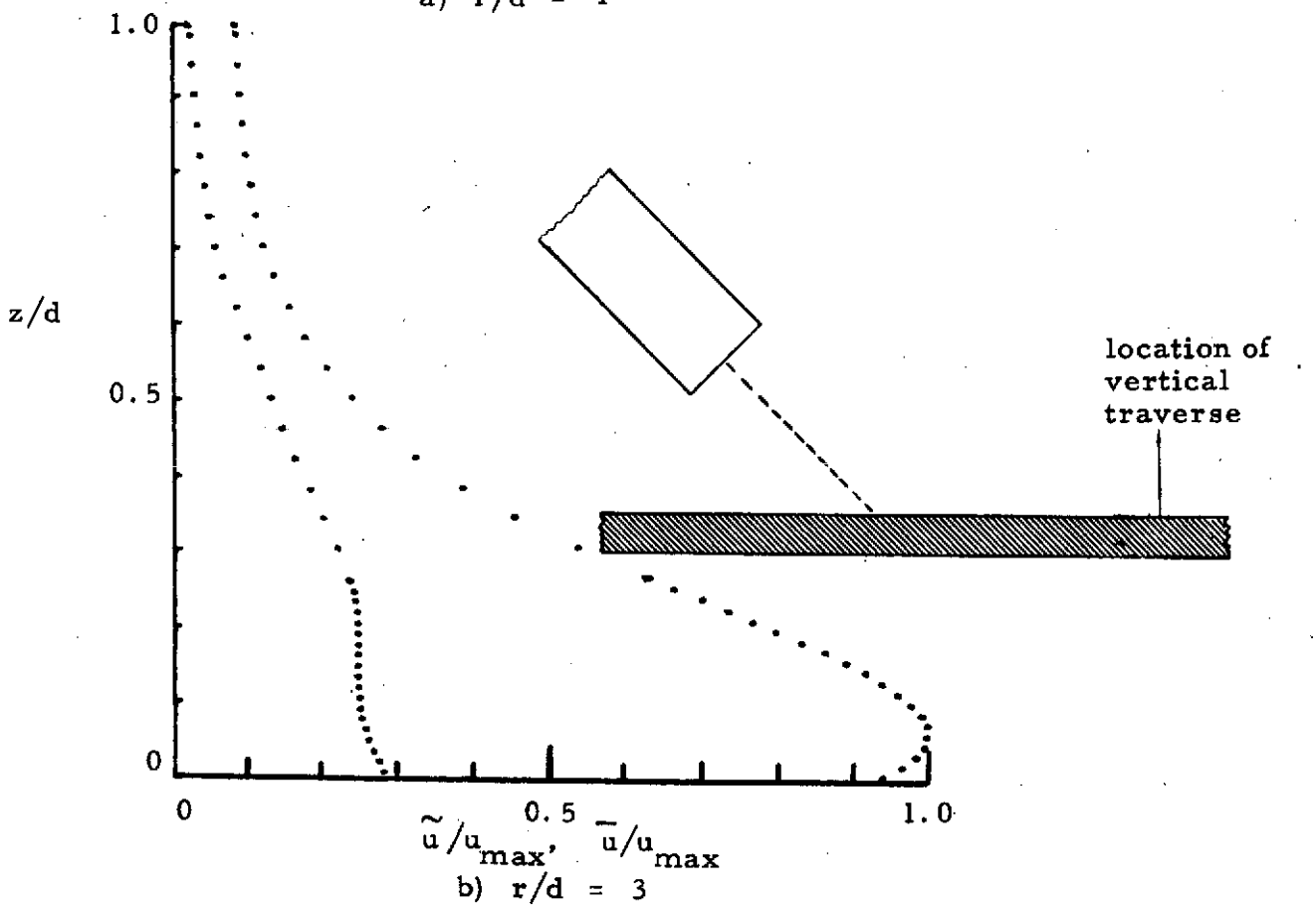

b) r/d = 3

Figure 35. Vertical traverse data.

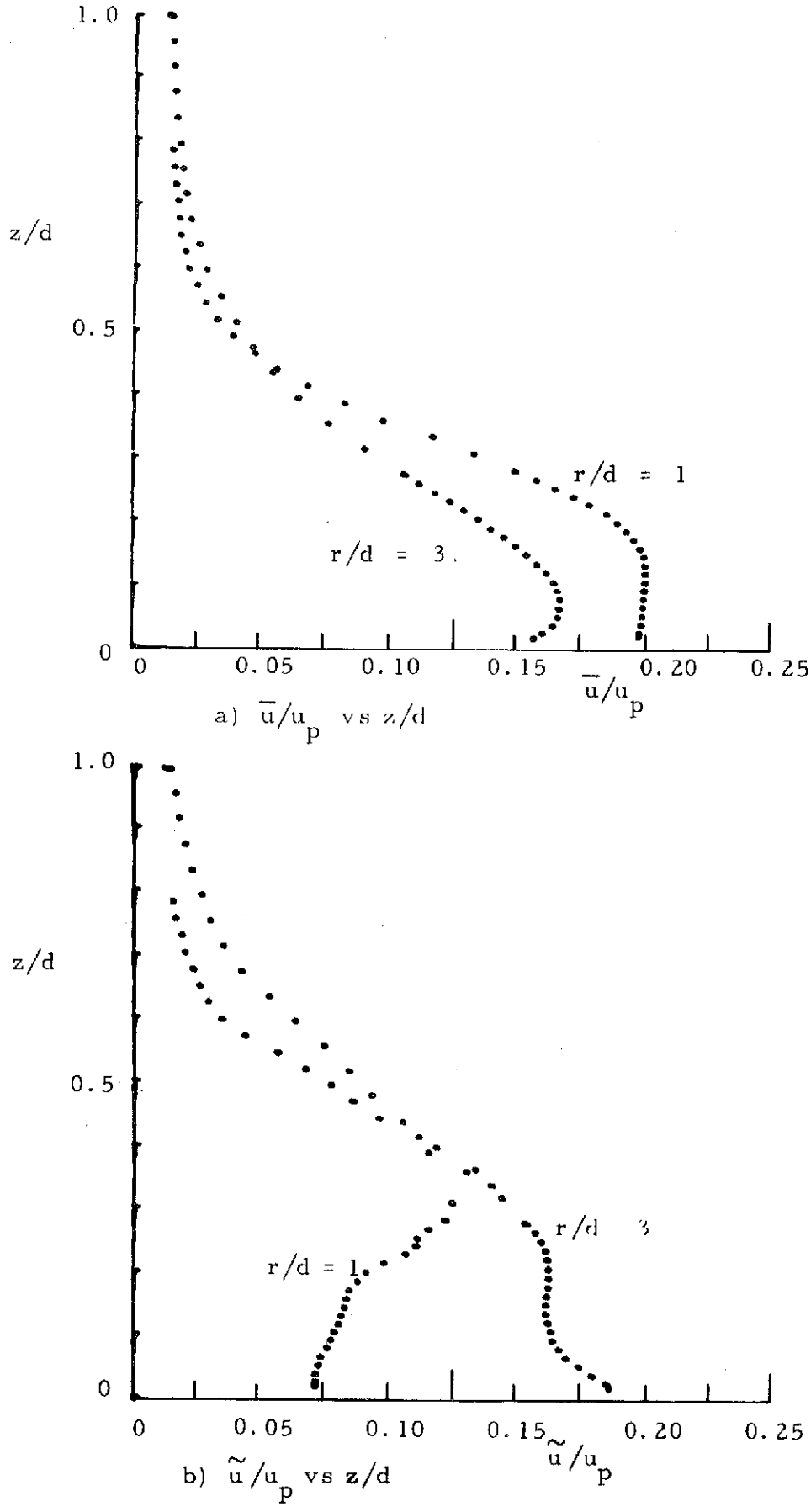

Figure 36. Comparison of vertical traverse data for r/d = 1 and 3.